© 2017. Published by The Company of Biologists Ltd | Journal of Cell Science (2017) 130, 2185-2195 doi:10.1242/jcs.203794

RESEARCH ARTICLE

The nuclear export factor CRM1 controls juxta-nuclear microtubule-dependent virus transport

I-Hsuan Wang[1,*,‡], Christoph J. Burckhardt[1,2,‡], Artur Yakimovich[1,‡], Matthias K. Morf[1,3] and Urs F. Greber[1,§]

ABSTRACT

Transport of large cargo through the cytoplasm requires motor proteins and polarized filaments. Viruses that replicate in the nucleus of post-mitotic cells use microtubules and the dynein–dynactin motor to traffic to the nuclear membrane and deliver their genome through nuclear pore complexes (NPCs) into the nucleus. How virus particles (virions) or cellular cargo are transferred from microtubules to the NPC is unknown. Here, we analyzed trafficking of incoming cytoplasmic adenoviruses by single-particle tracking and super-resolution microscopy. We provide evidence for a regulatory role of CRM1 (chromosome-region-maintenance-1; also known as XPO1, exportin-1) in juxta-nuclear microtubule-dependent adenovirus transport. Leptomycin B (LMB) abolishes nuclear targeting of adenovirus. It binds to CRM1, precludes CRM1–cargo binding and blocks signal-dependent nuclear export. LMB-inhibited CRM1 did not compete with adenovirus for binding to the nucleoporin Nup214 at the NPC. Instead, CRM1 inhibition selectively enhanced virion association with microtubules, and boosted virion motions on microtubules less than ∼2 µm from the nuclear membrane. The data show that the nucleus provides positional information for incoming virions to detach from microtubules, engage a slower microtubule-independent motility to the NPC and enhance infection.

KEY WORDS: Adenovirus, Fluorescence microscopy, Virus entry, Microtubule, Intracellular transport, CRM1, Machine learning

INTRODUCTION

The eukaryotic cytoplasm is a complex aqueous mixture of proteins, nucleic acids, solutes, and a range of membrane-limited organelles and membrane-free liquid-unmixed entities, such as stress granules, P-bodies and the pericentriolar matrix (Hyman et al., 2014; Mellman and Warren, 2000; Verkman, 2002). Efficient navigation of cargo, for example particles larger than 500 kDa, requires actin and microtubule filaments, and frequently the assistance of molecular motors stepping along the filaments in a polarized manner. Virus particles (virions) are larger than 20 nm in diameter, and require assistance to undertake the cytoplasmic motility that is necessary to cause infection (Dodding and Way, 2011; Greber and Way, 2006; Radtke et al., 2006). Infection involves motors that directly bind to virions, or move virions in endocytic or secretory vesicles (Greber and Way, 2006; Marsh and Helenius, 2006; Yamauchi and Greber, 2016). While short-range transport of virions often depends on actin and myosin motors (Taylor et al., 2011), long-range cytoplasmic transport requires microtubules, and, in the case of incoming virions, the minus-end-directed motor complex dynein–dynactin (Dodding and Way, 2011; Hsieh et al., 2010).

Like cellular cargo, viruses engage in bidirectional motor-dependent motility by recruiting cytoskeletal motors of opposite directionality (Greber and Way, 2006; Scherer and Vallee, 2011; Welte, 2004). The net transport balance of a cargo is determined at the level of motor recruitment, motor coordination and the tug-of-war between motors of opposite polarity, and also by post-translational modifications and changes in the dynamics of the microtubule tracks (Gross, 2004; Janke, 2014; Verhey and Gaertig, 2007). For example, low concentrations of tubulin-binding compounds stabilize microtubules, boost the nuclear accumulation and transcriptional activity of the tumor suppressor p53 (also known as TP53) and also enhance the rate of movement of fluorescent adenovirus to the nucleus (Giannakakou et al., 2002).

Adenovirus predominantly infects epithelial cells of the respiratory and gastrointestinal tracts, and conjunctiva (Robinson et al., 2013). The species C human adenoviruses (HAdV-C2 and -C5) are widespread, persist in adenoid tissue and are life-threatening to immune-compromised individuals (Lion, 2014). They enter epithelial cells by receptor-mediated endocytosis (Meier et al., 2002; Wolfrum and Greber, 2013), disrupt the endosomal membrane and escape as membrane-free particles into the cytosol (Luisoni et al., 2015; Moyer et al., 2011). The transport of adenovirus towards the microtubule-organizing center (MTOC, often located near the nucleus) depends on the dynein–dynactin motor complex (Bremner et al., 2009; Engelke et al., 2011; Kelkar et al., 2006, 2004; Leopold et al., 2000; Suomalainen et al., 1999). It is enhanced by cell signaling, such as p38 MAPK family signaling and protein kinase A (PKA) signaling pathways, which are activated by incoming virions (Wolfrum and Greber, 2013), together with the ERK1 and ERK2 pathway (ERK1/2, also known as MAPK3 and MAPK1, respectively) (Bruder and Kovesdi, 1997).

Remarkably, the direction of virion transport depends on the molecular composition of the particle. The incoming virion sheds accessory proteins in a stepwise manner during entry (Greber et al., 1993; Nakano et al., 2000). The cytosolic particles are leaky containers comprising the hexon protein and viral DNA, but lacking the pentons and some stabilizing proteins (Luisoni et al., 2015; Puntener et al., 2011; Wang et al., 2013). They are different from intact virions, which are regular icosahedral T=25 (where T is the triangular number, a standard way to describe the subunit number and organization of the facets of an icosahedron) particles of ∼90 nm in diameter (Liu et al., 2010; Reddy et al., 2010). When intact virions are experimentally delivered into the cytosol by needle-based microinjection, they are not transported to the nucleus,

[1]Department of Molecular Life Sciences, University of Zürich, 8057 Zurich, Switzerland. [2]Department of Bioinformatics, University of Texas Southwestern Medical Center at Dallas, Dallas, TX 75390, USA. [3]Molecular Life Sciences Graduate School, ETH and University of Zürich, 8057 Zurich, Switzerland.
*Present address: Division of Virology, Institute of Medical Science, the University of Tokyo, Tokyo 108-8639, Japan.
‡These authors contributed equally to this work

§Author for correspondence (urs.greber@imls.uzh.ch)

I.-H.W., 0000-0003-2159-7347; M.K.M., 0000-0001-7862-8322; U.F.G., 0000-0003-2278-120X

Received 10 March 2017; Accepted 12 May 2017

Journal of Cell Science

Journal of Cell Science (2017) 130, 2185-2195 doi:10.1242/jcs.203794

but towards the cell periphery, mimicking non-lytic virus egress from the infected cell (Suomalainen et al., 2001; Tollefson et al., 1996). This suggests that structural alterations in the virus particles and signaling induced by the incoming particles enable virion transport to the nuclear membrane. Besides activation of MAPK and PKA pathways, incoming adenovirus activates the Rac1 pathway, and thereby triggers viral endocytosis and macropinocytosis of fluids (Amstutz et al., 2008; Meier et al., 2002). Rac1 activation by incoming adenovirus leads to stabilization of microtubule dynamics and outgrowth of microtubules to the lamellar regions of cells, and enhances microtubule capture of cytosolic virions (Warren and Cassimeris, 2007; Warren et al., 2006).

How precisely adenovirus reaches the nuclear pore complex (NPC), where it delivers its genome into the nucleus only after minutes of docking at the NPC, has remained elusive (Berk, 2007; Cassany et al., 2014; Strunze et al., 2011; Trotman et al., 2001). Intriguingly, the nuclear export factor CRM1 (chromosome region maintenance 1), also known as XPO1 (exportin 1) has been implicated as a key player in adenovirus nuclear targeting (Smith et al., 2008; Strunze et al., 2005). CRM1 shuttles a large range of substrates bearing nuclear export sequences (NESs) from the nucleus to the cytoplasm, in association with the small GTP-binding protein Ran (Hutten and Kehlenbach, 2007; Kirli et al., 2015; Xu et al., 2015). Following treatment of cells with leptomycin B (LMB), which covalently binds to a cysteine residue in the central region of CRM1 and blocks the binding of NES-bearing cargo to CRM1 (Engelsma et al., 2004; Kudo et al., 1999; Neville and Rosbash, 1999; Sun et al., 2013), adenovirus no longer docks to the NPC. However, depending on the cell type, adenovirus is either arrested (stuck) at the MTOC or dispersed in the distal cytoplasm. The latter phenotype is observed for example in HeLa cells, which are known to have a distinct microtubule distribution (Li et al., 2012; Strunze et al., 2005; Wang et al., 2013). LMB precludes the uncoating and the delivery of viral DNA into the nucleus and blocks infection. Here, we used machine learning-based computer vision analysis to map the microtubule-dependent motions of adenovirus in the perinuclear region with high spatio-temporal resolution, and reveal a surprising function of nuclear export in regulating virion transport.

RESULTS

LMB-resistant CRM1 rescues nuclear targeting of adenovirus and restores infection in LMB-treated cells

CRM1 is the major export factor for leucine-rich NES-bearing proteins, and binds in a Ran-GTP-dependent manner to two cytoplasmic nucleoporins, Nup214 and Nup358 (also known as RANBP2) (Engelsma et al., 2004; Fornerod et al., 1997b; Hutten and Kehlenbach, 2006). Nup214 and Nup358 are required for adenovirus docking and uncoating at the NPC, respectively (Strunze et al., 2011; Trotman et al., 2001). LMB inactivates human CRM1 by covalent binding to cysteine 528 (C528), which is located in the NES-binding grove of CRM1. We first tested whether LMB-inhibited CRM1 interfered with adenovirus docking to the NPC in the presence of LMB. The expression of the LMB-resistant CRM1-C528S mutant (expressed as a CRM1–mCherry fusion protein, Hilliard et al., 2010) restored the cytoplasmic localization of the endogenous NES substrate Rio2 (also known as RIOK2, Zemp et al., 2009) in LMB-treated human embryonic retinoblast (HER)-911 cells (Fig. 1A,B). Expression of CRM1-C528S–mCherry gave rise to infection as measured by the expression of transgenic GFP from a replication-defective HAdV-C5 vector (Fig. 1A,B; Fig. S1). This was in stark contrast to non-transfected cells or cells expressing wild-type (wt)-CRM1–mCherry, which retained Rio2 in the nucleus upon LMB treatment and were resistant to infection. Infection, virion nuclear targeting and Rio2 nuclear export analyses in HeLa and HER-911 cells gave similar results (Fig. S1A–F). The subcellular distribution of incoming adenovirus particles was assessed through use of fluorescent HAdV-C2–Atto647. The majority of the virions (>60%) localized to the nucleus of control cells at 90 min post infection (mpi) (Fig. 1C,D). In LMB-treated cells expressing wt-CRM1–mCherry, the virions mostly accumulated at the MTOC, as indicated by pericentrin staining (Fig. S1G). The expression of CRM1-C528S–mCherry precluded virion accumulation at the MTOC, and significantly restored the nuclear localization of HAdV-C2–Atto647 (P=0.0041; Fig. 1C,D). A similar experiment with HAdV-C2 conjugated to Alexa Fluor 488 (HAdV-C2–Alexa488) in HeLa cells gave equivalent results; that is, a strong increase of virions targeted to the nucleus in LMB-treated cells expressing CRM1-C528S–mCherry compared to what was seen in cells expressing wt-CRM1–mCherry cells (P<0.0001; Fig. S1C,D). Taken together, these results show that the LMB-bound CRM1 does not block virion-docking sites at the NPC. This result was informative, since CRM1 and adenovirus use Nup214 as a docking site at the NPC (Cassany et al., 2014; Fornerod et al., 1997a; Trotman et al., 2001). The data imply that functional CRM1 is required for the nuclear targeting of adenovirus.

Inhibition of CRM1 increases microtubule-dependent motility of adenovirus

We examined whether CRM1 inhibition affected the cytoplasmic transport of adenovirus. For live-cell imaging, we used ultra-flat monkey kidney TC7 cells, and monitored the motion of fluorescently labeled HAdV-C2–Alexa488. TC7 cells that are infected by species C adenoviruses produce viruses in the absence of LMB, but in the presence of LMB, these cells accumulate incoming virions at the MTOC, akin to HER-911 cells (Staufenbiel et al., 1986; Strunze et al., 2005; Suomalainen et al., 1999). Virion motility in TC7 cells was determined by spinning disc confocal microscopy in the time window of 30–90 mpi. Cytosolic virions are the predominant entity in this time window, as indicated by previous studies showing that the half-time for virion penetration from endosomes is 15 min and that virions predominantly dock at the NPC after 30 min of infection (Engelke et al., 2011; Gastaldelli et al., 2008; Greber et al., 1997, 1993; Greber and Way, 2006; Imelli et al., 2009; Meier et al., 2002; Suomalainen et al., 2013, 2001; Trotman et al., 2001). Movies with a length of 200 s were recorded at an image acquisition rate of 25 frames per second (Hz). Virion trajectories were generated by single-particle-tracking algorithms (Fig. 2A), and further analyzed by machine-learning and motion segmentation techniques (Helmuth et al., 2007; Sbalzarini and Koumoutsakos, 2005). The location of the nucleus was determined by staining live cells with the fluorophore DRAQ5, and imaging along with virions (Fig. 2A, gray). For the assessment of cytoplasmic virion motility, the boundary of the nucleus was determined by image thresholding of the DRAQ5 nuclear signal (Fig. 2A, shown by a red line). The DRAQ5 thresholding is accurate, as indicated by a nearly perfect overlap of the nuclear border with POM121–GFP3, a marker of NPCs and the nuclear envelope (Fig. S2A; see Daigle et al., 2001). We conclude that DRAQ5 can be used to accurately determine the location of the nuclear envelope in live cells, here referred to as the ‘nuclear rim’. DRAQ5-stained nuclei hence serve as a reference site for the classification of subcellular virus motility.

We next validated the detection of virions by conducting a nuclear-targeting assay in live cells. Results show that LMB treatment of TC7 cells reduced the number of virions at the nuclear rim (Fig. 2B), in agreement with earlier results from chemically fixed HER-911 cells (shown in Fig. 1 and Strunze et al., 2005). Similar results were

Journal of Cell Science

Journal of Cell Science (2017) 130, 2185-2195 doi:10.1242/jcs.203794

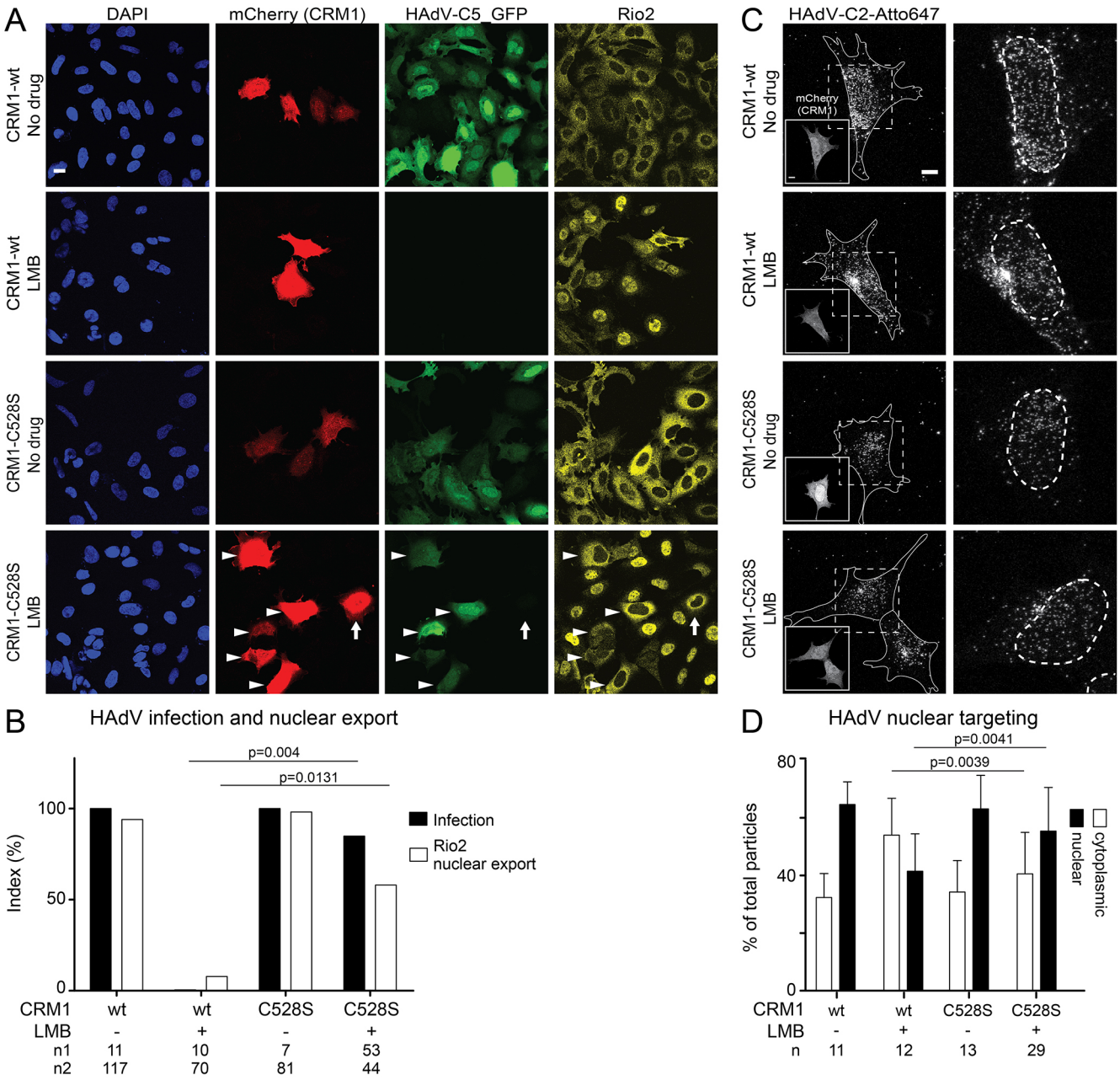

Fig. 1. Functional CRM1 is required for the nuclear targeting and genome delivery of adenovirus. (A) HER-911 cells transfected with CRM1-wt–mCherry or CRM1-C528S–mCherry were treated with or without LMB, infected with HAdV-C5_GFP for 16 h and analyzed for the endogenous CRM1 substrate Rio2. The expression of CRM1-C528S–mCherry rescued the nuclear export of Rio2 and HAdV-C5_GFP infection in LMB-treated cells (A, arrowheads), with only one exception in the representative image (arrow). Scale bar: 20 µm. (B) Mean infection indexes (percentage of GFP-positive cells, black bars) of transfected cells, and nuclear export indexes (white bars) obtained from two independent experiments, including the *P*-values from a t-test. The number of cells analyzed in each replicate is indicated (n1, n2). (C) Representative images of the nuclear targeting of HAdV-C2-Atto647 virions in the transfected cells at 90 mpi with and without LMB treatment. The expression of CRM1-wt–mCherry or CRM1-C528S–mCherry is shown in the white boxed insets, and the position of the nucleus is indicated by the dashed line in the magnified images. Scale bar: 10 µm. (D) Mean+s.d. values of the subcellular localization of virions at the nuclear membrane and in the cytoplasm. See also Fig. S1, which shows the results from HeLa cells.

obtained through live-cell imaging of HeLa cells, and revealed a strong increase in nuclear envelope targeting of virions between 0–30 mpi and 30–90 mpi (Fig. S2A–C). The increase of virions in very close proximity to the nuclear periphery was strongly reduced by LMB, indicating that the subcellular detection of virions by live-cell imaging is reliable and accurate (Fig. S2D).

We further characterized the virion motions by measuring the diffusion rate, speed, run length, duration and the moment scaling spectrum (MSS) slope of the trajectory elements. The MSS slope is a descriptor of the diffusive behavior, similar to the α coefficient of a mean square displacement plot (Ewers et al., 2005; Helmuth et al., 2007). MSS values below 0.5 indicate confined diffusion, values of 0.5 random walks and values above 0.5 diffusion with underlying drifts. Large data sets of several thousand trajectories for each condition showed that the overall diffusive motions of the viruses slightly increased upon LMB treatment of TC7 or HeLa cells, as indicated by the MSS slopes, the diffusion constants, the run lengths and the speeds (Fig. S2E–J). For example, the relative occurrence of

Journal of Cell Science (2017) 130, 2185-2195 doi:10.1242/jcs.203794

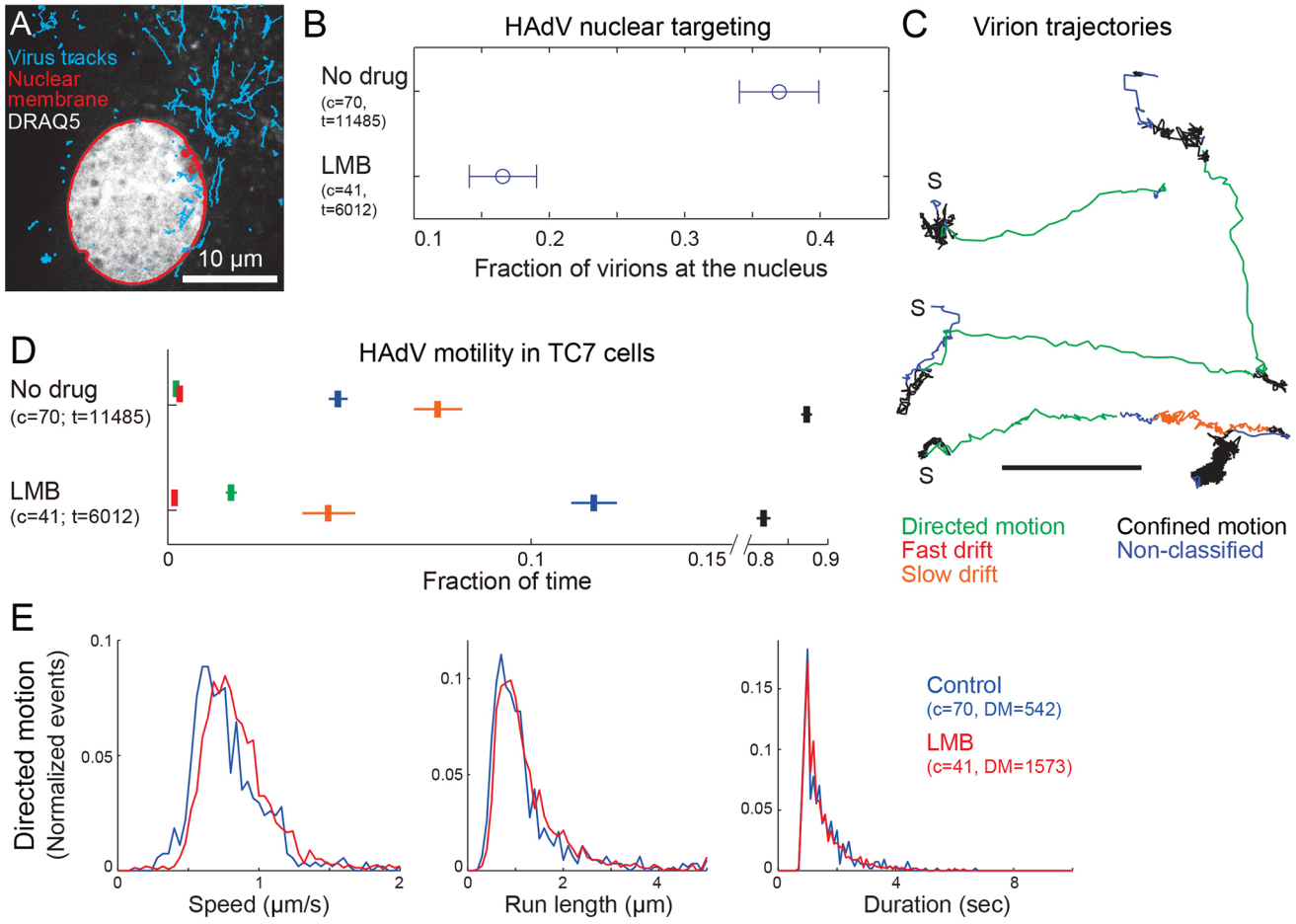

Fig. 2. CRM1 inhibition increases microtubule-dependent motility of adenovirus. (A) Virion trajectories (cyan) derived from 5000 time frames acquired at 25 Hz in TC7 cells infected with HAdV-C2–Alexa488. The position of the nuclear membrane is depicted in red, and has been derived from the DRAQ5 nuclear staining (gray). See also Fig. S2. (B) Analysis of nuclear targeting of adenovirus in the presence or absence of LMB, determined from the subcellular localization of virus tracks at 30–90 mpi. (C) Computational segmentation of virion trajectories into directed motion (green), fast drift (red), slow drift (orange), not classified (dark blue) or confined motion (black). Scale bar: 1 µm. S, start. (D) Analysis of the median time of virion engagement in each motion type. Color code as in C. Note that LMB enhanced the extent of directed motions. In B, the mean±s.e.m. is shown; in D, median±95% confidence intervals obtained by bootstrapping are shown; c indicates the number of cells, and t the number of virion trajectories analyzed. (E) Detailed characterization of the microtubule-dependent directed motion with determination of speed, run length and duration. Note that LMB slightly enhanced the speed and run length of DM. The number of cells (c) and DM segments analyzed are indicated. See also Figs S2, S3 and S4, which show the results from HeLa cells and the feature analyses of virus motions.

motion periods with an MSS slope larger than 0.5, that is, with a high component of drift, showed a relative increase upon LMB treatment of ∼4-fold in TC7 cells (3.6% versus 15.2%) and 1.3-fold in HeLa cells (9.2% versus 12.1%) (see Fig. S2E,H).

In the next step, we used a machine-learning approach to measure four specific features of the virus trajectories, directed motion (DM), fast drift (FD), slow drift (SD) and confined motion (CM) (Fig. 2C). In HeLa cells, DM segments have speeds of 0.2 to 2 µm/s and run lengths of 0.4 up to 7 µm, while FD segments were slower (0.02 to 0.4 µm/s) and shorter (0.05–2.5 µm) (Engelke et al., 2011). Both DM and FD were abolished by depolymerization of microtubules with nocodazole, as reported previously (Engelke et al., 2011; Helmuth et al., 2007), and confirmed here (Fig. S2K). In control TC7 cells, the viruses spent 0.24% of the trajectory time in DM and 0.34% in FD motion (Fig. 2D). LMB treatment significantly increased the motility of the virions (Movie 1). In particular, LMB increased DM to 1.75%, and reduced CM to 81.9% compared to 87.3% in the control cells. In addition, LMB increased the speed and the run length of individual DM segments, but not the duration, and LMB had little effects on FD, SD or CM, as indicated by large-scale analyses (Fig. 2E; Fig. S3). These results show that in CRM1-inhibited cells, adenovirus remains engaged with microtubule-dependent fast transport, which, for example, can be mediated by the dynein–dynactin motor complex.

A CRM1-dependent gradient of adenovirus motility on microtubules close to the nuclear membrane

To assess whether CRM1 inhibition affected the directionality of DM segments in TC7 cells, we analyzed hundreds of DM segments in different subcellular regions. Directionality of the DM segments in the TC7 or HeLa cytoplasm outside the perinuclear area or around the MTOC was independent of LMB (Fig. 3A,B; Figs S3A–C and S4). DM segments towards and away from the nucleus were broadly similar in frequency, speed, length and duration (Fig. 3C). This makes it unlikely that LMB leads to virion accumulation at the MTOC by selective inhibition of the periphery-directed virion motions.

Similar observations were made in HeLa cells (Figs S2B,H–J, S4). These cells are known to transport the adenovirus particles less rapidly to the cell nucleus than the TC7 cells do, and do not enrich the virions at the MTOC upon LMB treatment (Strunze et al.,

Journal of Cell Science (2017) 130, 2185-2195 doi:10.1242/jcs.203794

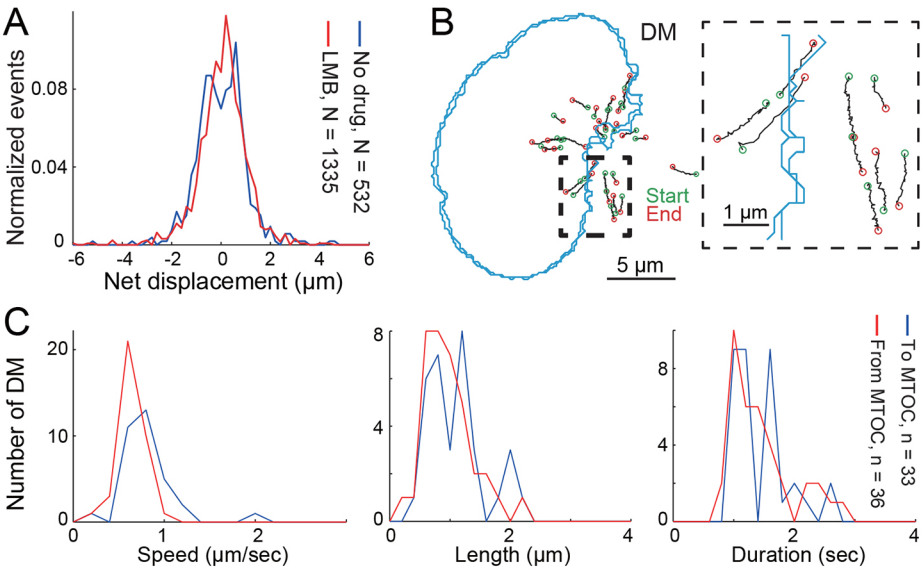

Fig. 3. No apparent bias in the directionality of adenovirus transport in the cytoplasm of LMB-treated cells. (A) Histogram depicting the net displacement of directed motions (DM) segments towards the nucleus (negative values) and away from the nucleus (positive values). N indicates the number of DM analyzed in control and LMB-treated TC7 cells infected with HAdV-C2–Alexa488. (B) No apparent preference of directed motions towards or away from the MTOC in LMB-treated cells. Green circles indicate the start-point and red circles the end-point of a DM which is depicted by a black line. (C) Detailed characterization of DM towards the MTOC (blue), and away from the MTOC (red) in LMB-treated TC7 cells, depicting speed, length and duration. *n*=3 cells were analyzed. *n* indicates the number of DM segments analyzed.

2005; Suomalainen et al., 1999). This is in agreement with the observation that LMB increased FD motion rather than DM in HeLa cells (Fig. S5). Taken together, the data suggest that CRM1 or a CRM1 export cargo does not affect the transport directionality of virions, but reduces microtubule-dependent viral motions, and may play a role in uncoupling the virions from MT-dependent transport.

CRM1 alone and in complex with export cargo is kinetically enriched around the nuclear membrane rather than being enriched in the cytoplasm or the nucleoplasm (Daelemans et al., 2005). We found that in control cells, virions were enriched over the nuclear periphery bound to NPCs, and depleted in a zone of 3–4 μm around the nuclear membrane, as indicated by distance distribution plots of the virus residence time (Fig. 4A). In CRM1-inhibited cells, however, only a few virions were observed over the nucleus, as expected. Strikingly, LMB treatment enriched virus tracks in the close proximity of the nucleus, particularly in the cytoplasmic area 1–3 μm from the nuclear rim, as indicated by residence time measurements (Fig. 4A, arrow). Virion tracks occurred all over the cytoplasm, and contained the previously detected features, DM, FD, SD and CM segments (Fig. 4B). We closely analyzed those viral trajectories that contained at least one segment of microtubule-dependent motions, either DM or FD, diagnostic features of microtubule-dependent tracks.

There was no significant difference in DM or FD between LMB and control cells in cytoplasmic regions more than 1.6 μm from the nucleus (Fig. 4C). However, control cells exhibited reduced occurrence of DM in close vicinity, within –1.6 μm to +1 μm, of the nuclear rim (Fig. 4D). This gradient of microtubule-dependent motions around the nuclear rim was absent in the LMB-treated cells, which showed a quasi-uniform DM frequency around the nucleus. A similar gradient in control but not LMB cells was detected for nonclassified motions, which comprise shorter and less directional motions than DM (Helmuth et al., 2007).

These findings were supported by the observation that LMB shifted the starting points of DM segments to locations close to the nuclear rim, in most cases closer than 5 μm, which is distinct from what is observed in control cells where DM was initiated up to 20 μm away from the nuclear rim (Fig. 4D). The LMB-treated cells contained virtually no detectable SD, in stark contrast to what is seen in the control cells, which contained high amounts of these microtubule-independent motions in the nuclear rim area, covering ∼1 μm over both the nuclear membrane and the adjacent cytoplasm, indicative of virions attached to NPCs (Fig. 4C). Analyses in HeLa cells gave similar overall results, although the effects of LMB were not as pronounced as in TC7 cells, most likely since HeLa cells exhibit less extensive microtubule-dependent motions than TC7 cells (Fig. S5A,B).

Collectively, the results reveal that virions engaged infrequently with microtubule-dependent transport in the immediate proximity of the nucleus, unlike in other regions of the cytoplasm. Instead, the nucleus-proximal virions underwent slower motions and thereby sustained their drift, and eventually anchored at the NPC, as indicated by confined motions. Upon CRM1 inhibition, nucleus-proximal virions did not uncouple from microtubule-dependent transport near the nuclear rim, but kept moving through DM and fast non-classified motions. These virions engaged rarely in confined motions, and did not bind to the NPCs, but eventually became enriched at the MTOC as misdelivered particles.

CRM1 inhibition promotes adenovirus association with microtubules proximal to the nucleus

We next tested whether LMB enhanced the location of virions on microtubules near the nuclear rim of HER-911 cells. HER-911 cells are known to enrich the incoming adenovirus particles at the MTOC upon LMB treatment, very much like the TC7 cells (Strunze et al., 2005). HER-911 cells have a perinuclear microtubule network, which is accessible to analyses by super-resolution fluorescence microscopy. To obtain super-resolution, we used the gated-stimulated emission depletion microscopy (gSTED) in 3D mode, with spatial resolution of ∼135 nm in both *x*-*y* and *z* dimensions (Fig. 5A). All virions located closer than 1 μm to a microtubule were included in the profiling analysis of the perinuclear cytoplasm up to a distance 2.4 μm from the nuclear rim. Of note, virions that clustered at the MTOC were not analyzed, since their density was too high to be resolved by gSTED in 3D mode. For reference staining of MTOC with anti-pericentrin antibodies in HER-911 cells and frequency analyses of MTOC location with respect to the nuclear rim, see Figs S6A,B and S1G. This procedure allowed us to score those virions that were located in the perinuclear area but not bound to NPCs (data not shown). The distance between a virion and the nearest microtubule was

Journal of Cell Science (2017) 130, 2185-2195 doi:10.1242/jcs.203794

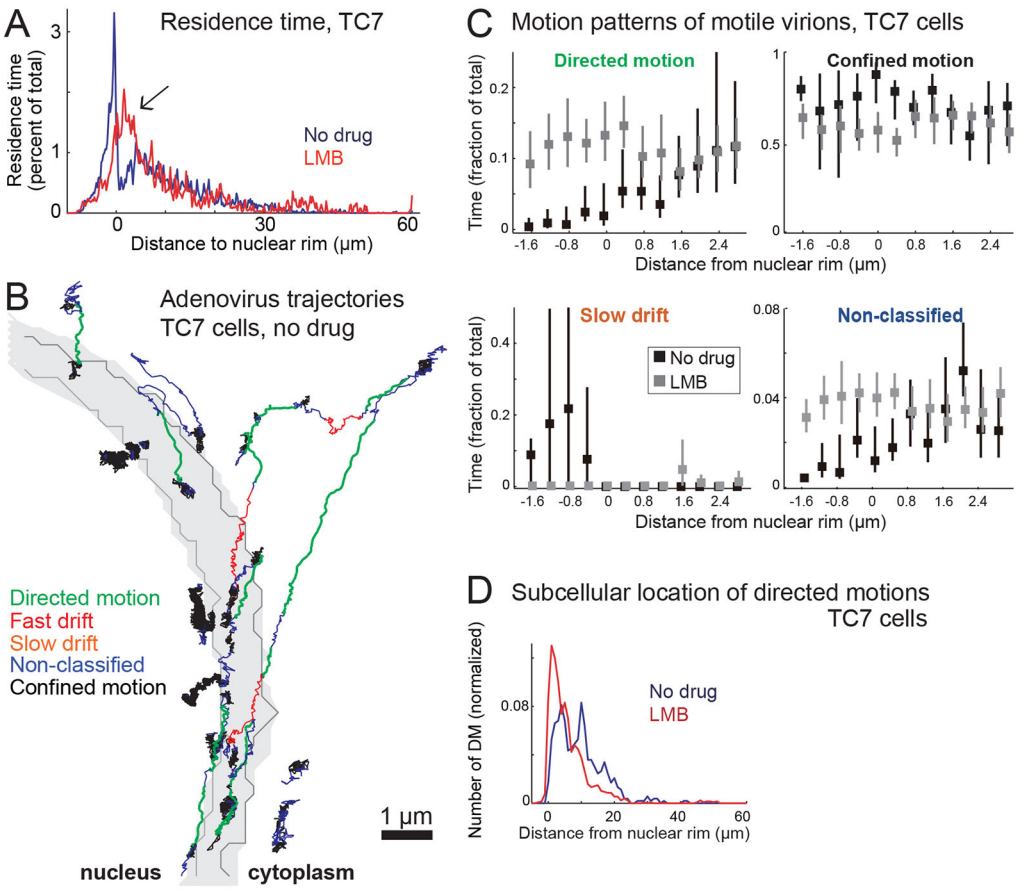

Fig. 4. CRM1-sensitive motion gradients of adenovirus at the nuclear membrane. (A) Analysis of spatially resolved virion residence time in TC7 cells infected with HAdV-C2–Alexa488 with or without LMB in the time window 30–90 mpi. Note the enhanced location of virions at the nuclear membrane in control cells (blue peak at position 0), and at a nucleus-proximal position in LMB-treated cells (red peak at position at 1–3 µm, black arrow). For control cells, we analyzed 70 cells with 3.4 million virus positions, and for LMB-treatment 41 cells with 8.7 million positions. (B) Segmentation of virion trajectories reveals directed motion (green), fast drift (red), slow drift (orange), confined motions (black) or not classified (dark blue) trajectories near the nuclear rim. The nuclear rim zone is depicted in gray as a curved area. (C) Spatially resolved analysis of the median residence time (±95% confidence intervals obtained by bootstrapping) of virion motions shows a gradient of directed motions and non-classified motions, from –1.6 to 2.4 µm, in the perinuclear region. The nuclear rim is located at 0 µm. Each motion step in the respective segments was classified according to its localization. (D) Directed motions shifted from the cell periphery to the perinuclear region by LMB treatment, as indicated by frequency plots using the start of the motion as a reference point. See also Fig. S5, which shows the results from HeLa cells.

determined and plotted in relation to the distance from the nuclear rim (Fig. 5B).

We found that the average distance of the virions from microtubules most proximal to the nuclear rim (0 to 0.4 µm) was reduced by more than 2-fold in LMB-treated cells compared to what was seen in the control cells. There was no difference in virion location with respect to microtubules in the more distal regions of the cell. Similar results were found in frequency plots of virion distances from microtubules (Fig. 5C). They demonstrate that the nuclear rim zone (≤1 or >1 µm from the nuclear membrane) in LMB-treated cells contained more than twice the proportion of virions than were less than ∼100 nm away from a microtubule (red line), compared to what was seen in control cells (dark blue, P=0.003). The nuclear rim zone of LMB cells but not control cells also contained a higher proportion of virions closer to microtubules than the rest of the cytoplasmic area (P-values of 0.013 and 0.09, respectively, see Fig. 5C). Similar to the results with HER-911 cells, we also found an overall enhancement of virion association with microtubules in HeLa cells upon LMB treatment (data not shown). However, we could not detect any gross changes in the density or the arrangement of microtubules in the nucleus-proximal region (3 µm) in HER-911 or HeLa cells (Fig. S6C–E). The results show that CRM1 inhibition retains virions on microtubules near the nucleus.

DISCUSSION

Virus entry into cells requires an extensive array of host proteins, lipids and solutes. Conceptually, information flows from the incoming virus particle to the cell, and backwards from the cell to the virion (Wolfrum and Greber, 2013). Here, we provide novel evidence for information flow from the nucleus to virions moving on microtubules proximal to the nucleus. Viruses replicating in the nucleus, such as influenza, papilloma, polyoma and human foamy virus are transported towards the nucleus within vesicles, and release their genome in the proximity of the nucleus, whereas others use bidirectional transport of nucleocapsids on microtubules for the nuclear delivery of their genomes through the NPC, such as human immune deficiency virus, herpes virus, parvovirus, hepatitis B virus and adenovirus (reviewed in Aydin and Schelhaas, 2016; Dodding and Way, 2011; Greber and Way, 2006; Hsieh et al., 2010; Trobridge, 2009). The steps required for virus transfer from microtubules to the nuclear pores are unknown.

Our findings reveal three novel aspects of microtubule-dependent transport. First, we demonstrate that fast bi-directional virion

Journal of Cell Science (2017) 130, 2185-2195 doi:10.1242/jcs.203794

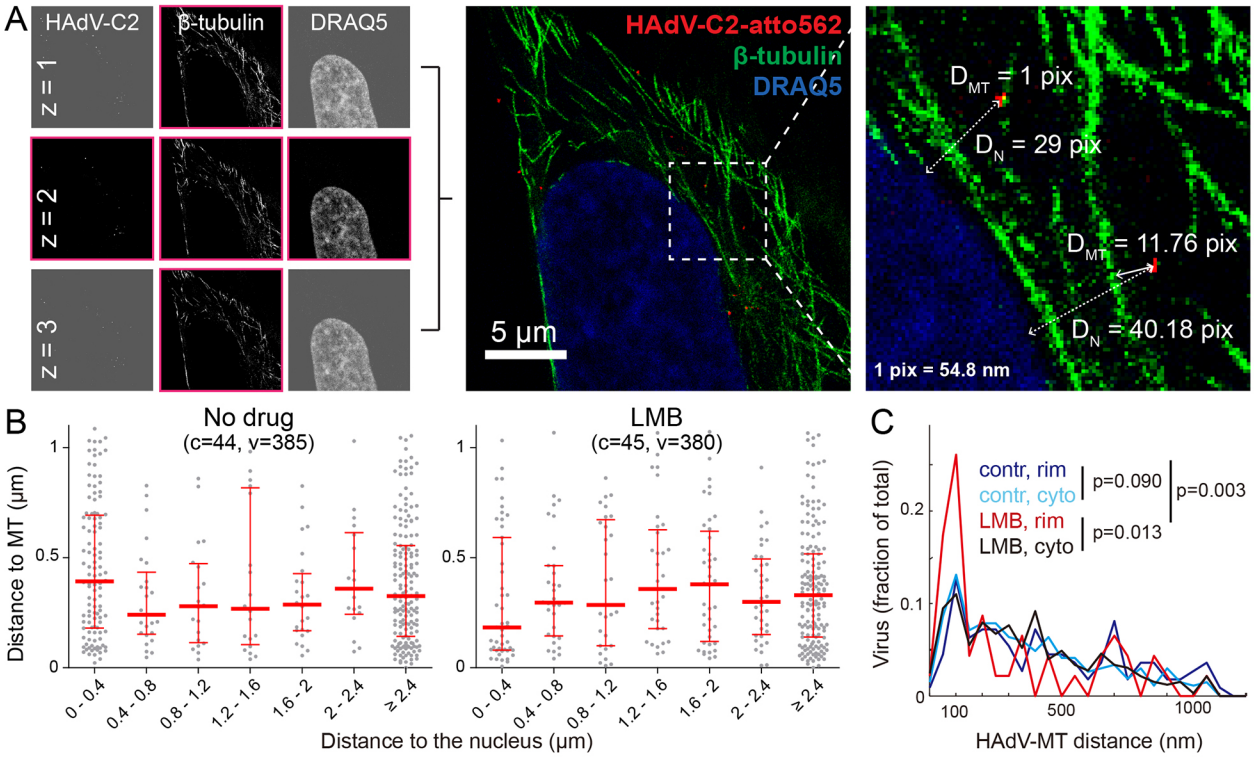

Fig. 5. LMB reduces the distance of adenovirus particles to microtubules in immediate surroundings of the nuclear membrane. (A) HER-911 cells were infected with HAdV-C2–Atto565 (red) in the presence or absence of LMB for 60 or 90 min, fixed, and stained for β-tubulin (green) and nuclei (DRAQ5; blue). gSTED stacks including three *z*-sections were acquired for virus, microtubules and the nucleus. The middle sections (z=2) are shown in the raw gray scale, and were used to locate virions and the nuclear rim. All three tubulin sections were used to locate microtubules to enhance accuracy of virion proximity location. Sections 1 and 3, depicting virions and nuclei, are shown in artificial gray tone, and were not used for analyses. With this procedure, the distance of each virion to the closest microtubule (D_{MT}) and the nuclear rim (D_N) was determined. An example image is shown in the right-most panel. (B) Frequency analysis of virion distance to the nearest microtubule as a function of subcellular location. Red lines indicate the median value and the interquartile range. The bin size of the data is 0.4 µm except for the last bin, which contains all virions located 2.4 µm and further away from the nucleus. Virions located closer then 110 nm were classified as colocalizing with a microtubule. The number of cells (c) and virions (v) are indicated for control and LMB-treated cells. (C) Profiling of the virion distance to the nearest microtubule in the nuclear rim area (1 µm each over the nuclear membrane and the adjacent cytoplasm) and in the more distant cytoplasm (cyto) shows that LMB enhances the fraction of virions located at less than 100 nm from the nearest microtubule. Statistical analyses and *P*-values for the D_{MT} distribution were obtained by performing a Kolmogorow–Smirnov test. See also Fig. S6 for the subcellular localization of the MTOC and the morphology of perinuclear microtubules.

transport on microtubules is reduced in the immediate proximity of the nuclear membrane compared to in other regions in the cytoplasm. Second, we show that virions in the immediate proximity of the nucleus are detached from microtubules. Third, both observations are critically dependent on functional nuclear export through the exportin CRM1, as shown by the use of the specific CRM1 inhibitor LMB, which binds to CRM1 and precludes CRM1 association with NES-bearing cargo and hence Ran-GTP binding (Engelsma et al., 2004; Kudo et al., 1999; Neville and Rosbash, 1999). We also noted that the LMB treatment increased the fraction of microtubule-dependent motions across the entire cell (Fig. 2D; Fig. S3A, Movie 1).

CRM1 was previously shown to be required for the attachment of incoming adenovirus particles to NPCs (Strunze et al., 2005). Our data here support a model where CRM1 enhances the unloading from or inhibits the loading of virions to microtubules. This enables virion access to the NPC for uncoating and nuclear delivery of the viral genome, as depicted in Fig. 6. We can rule out that the LMB-inhibited CRM1 competes with virion for docking at the NPC, consistent with the notion that the phenylalanine-glycine repeats in the N-terminal domain of Nup214 are used for adenovirus binding but not for CRM1 interactions (Cassany et al., 2014; Fornerod et al., 1997b; Napetschnig et al., 2007).

Our study uncovers, for the first time, a gradient of microtubule-dependent motions of a cargo in the nucleus-proximal cytoplasm. The motion gradient of adenovirus particles extended ∼2 µm from the nuclear membrane to the cytoplasm, and the gradient was completely abrogated by inhibition of CRM1-dependent nuclear export. It is less likely that CRM1 or CRM1–Ran-GTP compete with motors for virion binding, since neither recombinant CRM1 nor CRM1–Ran-GTP were found to bind to purified adenovirus particles (Markus Eisenhut and U.F.G., data not shown).

The molecular nature of the unloading factor or the factor precluding rebinding of adenovirus to the nucleus-proximal microtubules remains unknown. A recent study identified a rather large number of proteins, in the range of 1000, that are subject to CRM1-mediated export from yeast, frog or human cell nuclei (Kirli et al., 2015). One possible explanation for the adenovirus motion gradient is that a CRM1 export substrate alone or a complex of CRM1–Ran-GTP detaches the motors bound to the virion from the microtubules near the nucleus. For example, microtubule binding of the kinesin-1 motor could be regulated by nuclear export of histone deacetylases (HDACs). Kinesin-1 preferentially binds to and translocates on acetylated and detyrosinated microtubules (Reed et al., 2006). In cultured epithelial cells, these features occur on microtubules in the perinuclear region, and confer a predominantly

Journal of Cell Science (2017) 130, 2185-2195 doi:10.1242/jcs.203794

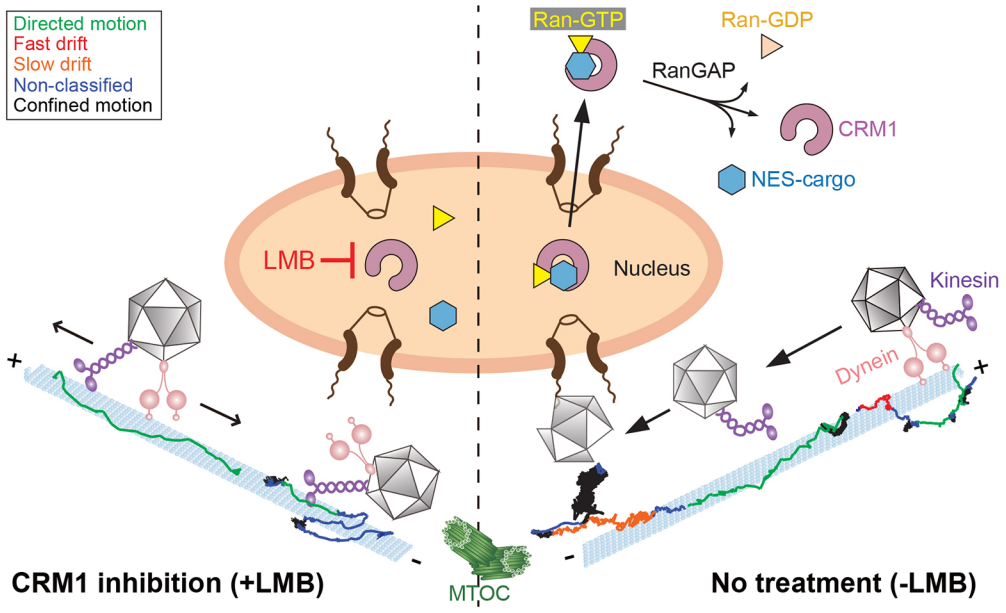

Fig. 6. Model for CRM1-regulated adenovirus association with MT-dependent transport. Incoming adenovirus particles are transported on microtubules towards the nucleus by the dynein–dynactin motor complex, and an unidentified plus-end-directed motor, such as kinesin (Bremner et al., 2009; Suomalainen et al., 1999). The study here identified a motion gradient of adenovirus in the immediate cytoplasmic vicinity of the nucleus (~1 µm from the nuclear membrane). In this zone, the microtubule-dependent virion motility was strongly reduced, and the virion distance to the nearest microtubule strongly increased. These motility and location gradients were disrupted in cells treated with the nuclear export inhibitor LMB. The data argue that there are one or more spatial cues that uncouple the incoming virions from microtubules in the immediate proximity of the nuclear membrane and enable virion docking to the nuclear pore complex. At the NPC, the virion disassembles because of a cue from activated kinesin-1, which displaces capsid fragments to the distal cytoplasm, and allows viral DNA import into the nucleus (Strunze et al., 2011; Trotman et al., 2001).

stable state of microtubules, with a propensity to bend and curve (Friedman et al., 2010; Piperno et al., 1987; Schulze et al., 1987). HDACs could reduce the perinuclear acetylated α-tubulin levels, and thereby lower the interaction of microtubules with kinesin-1. Another CRM1 nuclear export substrate modulating microtubule-dependent motor movements is the tubulin deglutamylase CCP1 (also known as AGTPBP1) (Kirli et al., 2015; Thakar et al., 2013). Polyglutamylated yeast microtubules enhance the run lengths of kinesin-1, and, in flagella, long polyglutamate side-chains enhance dynein motility (Kubo et al., 2010; Sirajuddin et al., 2014). Hence, deglutamylation of nucleus-proximal microtubules could reduce the transport of cargo, such as adenovirus particles.

Alternatively, a CRM1 export substrate or a complex of CRM1, Ran-GTP and the export substrate may inhibit the rebinding of virion–motor complexes to microtubules in the nuclear vicinity, for example the dynein–dynactin complex. In support of the CRM1–Ran-GTP–export-substrate gradient hypothesis, a cytoplasmic Ran-GTP gradient over a few micrometers has been measured around condensed chromosomes of mitotic cells, and a Ran-GTP gradient of 0.5 to 2 µm around the nuclear membrane has been suggested for interphase cells based on mathematical modeling (Becskei and Mattaj, 2003; Görlich et al., 2003; Kaláb et al., 2006; Smith et al., 2002).

Our segmentation of virion motions based on machine learning further revealed a set of slower microtubule-independent drifting motions in the immediate vicinity of the nuclear membrane. These motions were suppressed by LMB. They are distinct from random walks, and imply a microtubule-independent transport machinery populating the perinuclear ecology. They may be similar to observations with HIV, which engages in rapid and directional microtubule-dependent motions, and also slower and possibly actin-dependent motions (Arhel et al., 2006; McDonald et al., 2002). These slow motions may be key for bringing the virions to the NPCs, and complement the fast adenovirus motions on microtubules, which are part of the perinuclear ecology (Mahamid et al., 2016).

We speculate that adenovirus particles require a particularly high concentration of motors to move on microtubules. The motors bind rather weakly and in low copy numbers to the adenovirus particles (Bremner et al., 2009; Gazzola et al., 2009). Accordingly, microtubule-dependent adenovirus motion bursts are rare, amounting to a few percent of the life time of the virions in the cytosol (Engelke et al., 2011; Helmuth et al., 2007). These features may render the virions particularly sensitive to spatial cues from the nucleus. This situation may occur for viruses with low frequency motion bursts, while other viruses with more frequent motion bursts may be less sensitive to microtubule detachment cues, such as herpes simplex virus, which stably engages with microtubule motors and is transported over long distances (Ekstrand et al., 2008; Greber and Way, 2006; Radtke et al., 2010).

MATERIALS AND METHODS

Cells and viruses

HeLa-K cells (provided by Ulrike Kutay, ETH Zurich, Switzerland), human epithelial KB cells (obtained from American Type Culture Collection), adenovirus-transformed human embryonic retinoblasts 911 cells (Fallaux et al., 1996) and TC7 cells (Suomalainen et al., 1999) were grown at 37°C under 5% CO_2 in the growth medium [Dulbecco's modified Eagle's medium (DMEM) supplemented with 5% fetal calf serum (FCS) and 1% non-essential amino acids (Gibco-BRL)]. Wild-type HAdV-C2 was grown in KB cells, and isolated and subsequently labeled with Atto565, Alexa Fluor 488 or Atto647 (ATTO-TEC GmbH, Siegen, Germany) as described previously (Greber et al., 1998). HAdV-C5_GFP was grown in HER-911 cells complementing the E1 region of adenovirus. HAdV-C5_GFP is a non-replicating virus expressing enhanced GFP in the E1 region under the cytomegalovirus (CMV) major immediate early promoter (Nagel et al., 2003). Both viruses were purified by equilibrium centrifugation over two

Journal of Cell Science (2017) 130, 2185-2195 doi:10.1242/jcs.203794

subsequent CsCl gradients, and their protein concentrations were measured with the Pierce Micro bicinchoninic acid (BCA) protein assay reagent kit (Thermo Fisher Scientific, Lausanne, Switzerland) (Greber et al., 1993).

Antibodies, plasmids and chemicals

Mouse monoclonal anti-β-tubulin antibody (1:250–1:500; N357) was purchased from Amersham (GE Healthcare, UK). Rabbit anti-pericentrin antibody (1:1000–1:2000; ab4448) was bought from Abcam (Cambridge, UK). Rabbit anti-Rio2 antibody was kindly provided by Ulrike Kutay (ETH, Zurich, Switzerland) (Zemp et al., 2009). Goat anti-rabbit- or goat anti-mouse-IgG coupled to Alexa Fluor 488, 594 or 633 were purchased from Life Technologies (Carlsbad, USA). Hemagglutinin (HA)-tagged CRM1 and CRM1-C528S expression plasmids were kindly provided by Ralph Kehlenbach (University of Göttingen; Hilliard et al., 2010). For this study, the HA tags of the CRM1 constructs were replaced by the fluorescent protein mCherry using the BamH1 and Xba1 restriction sites. The expression construct rPOM121-EGFP3 was obtained from Jan Ellenberg (EMBL, Heidelberg, Germany). Transient transfections were performed with either JetPEI (Polyplus-transfection SA, France) or electroporation using the Neon Transfection System (Life Technologies, USA), or BTX T820 Electro Square Porator (BTX Instrument Division, Harvard Apparatus, Inc., USA). LMB was purchased from LC laboratories (Woburn, USA), and stored in ethanol at –20°C until use.

Virus infection

Cells were seeded on coverslips in 12- or 24-well dishes and grown to 60–80% density for 1–2 days. HER-911 cells were treated with or without 20 nM LMB for 30 min, pulse infected with fluorescent HAdV-C2 (0.1 µg of virus per well, yielding about 50 to 300 internalized viruses per cell) at 37°C for 15 min in growth medium. Synchronized infection of HeLa or TC7 cells was performed by binding virus on ice for 1 h in the RPMI medium (Sigma-Aldrich) supplemented with 0.2% bovine serum albumin (BSA) (Suomalainen et al., 1999). The inoculum was removed, and cells were washed once with pre-warmed growth medium and further incubated at 37°C with or without 20 nM LMB as indicated. Transgene expression from HAdV-C5_GFP was measured by continuous incubation of cells with 24 ng of virus at 37°C for 16 h in growth medium, in the presence or absence of 20 nM LMB.

Immunocytochemistry

Samples were fixed in 4% paraformaldehyde for 15 min. For staining of microtubules, the fixation was performed with PHEMO-fix (3.7% formaldehyde, 0.05% glutaraldehyde, and 0.5% saponin in PHEMO-buffer, which contains 68 mM PIPES pH 6.9, 25 mM HEPES, 15 mM EGTA, 3 mM $MgCl_2$ and 10% DMSO) for 10 min (Mabit et al., 2002). Samples were quenched with 25 mM ammonium chloride, permeabilized with 0.5% Triton X-100 at room temperature, labeled with primary antibodies and the fluorophore-conjugated secondary antibodies. The cellular DNA was stained with either 4′,6-diamidino-2-phenylindole (DAPI, Molecular Probes, Leiden, The Netherlands) or DRAQ5 (Cell Signaling Technology, Inc., Massachusetts, USA). The samples were mounted in DAKO medium (Dako Schweiz AG, Baar, Switzerland) for regular confocal microscopy, or in ProLong Gold antifade reagent (Life Technologies, Carlsbad, USA) for super-resolution microscopy.

Image acquisition and analysis for end-point assays

Adenovirus infection and nuclear targeting were imaged with a Leica SP5 confocal laser-scanning microscope. HAdV-C5_GFP infection was determined by measuring the average intensity of the GFP signal over the nuclear area defined by the DAPI stain. To quantify the nuclear export, average Rio2 intensities were measured at the nuclear area and a 0.8-µm-wide rim region in the cytoplasm adjacent to the nucleus. The nuclear export efficiency was defined as the ratio of the average Rio2 intensity at the nuclear region divided by the average intensity in the rim region. Nuclear targeting of incoming adenovirus was determined through acquisition of image stacks with 0.5 µm *z*-step. Maximum projections of each image stack were processed by adaptive local thresholding to generate masks for each particle in the virus images and for nuclei in DAPI images. The virus masks were used to measure total fluorescence intensities over the particle areas (‘particle intensity’). The nuclear region was defined by the nucleus mask plus an extension of 0.4 µm towards the cytoplasm. The cell boundary was determined manually from cytoplasmic autofluorescence in computationally overexposed images. The cytoplasmic region was set as the region between the nuclear rim and the cell boundary. Nuclear targeting efficiency was expressed as percentage of total particle intensity in the nuclear area.

The subcellular location of the MTOC was analyzed in 96-well black plate samples (Greiner Bio-One GmbH, Frickenhausen, Germany). Image acquisition was performed with an automated ImageXpress Micro XLS wide-field fluorescence microscope (Molecular Devices, CA, USA) equipped with a 100× air objective (numerical aperture 0.9). The MTOC signal located outside of the DAPI mask was identified, and its distance to the nucleus determined.

To analyze the HAdV localization with respect to microtubules, super-resolution images were acquired with a Leica TCS SP8 STED 3X super-resolution microscope using a 100× oil immersion objective (numerical aperture 1.4). All STED images were acquired in the 3D gSTED mode with a pixel size of 54.8 nm, with an effective resolution estimated to be ∼135 nm in both *x*-*y* and *z* dimensions. During the image acquisition, the microscope was focused to the region of interest in the virus channel. While the DRAQ5 channel was imaged at the same focal plane as the viruses, a *z*-stack of three images centered at the focal plane was acquired in the microtubule channel with 70 nm *z*-steps. The distances between the virions and the nucleus, and between the virions and the closest microtubule were measured within the single section of the virus and DRAQ5 images, and in the maximum projection of the MT image stack. The effective resolution here was estimated from the average full width at half maximum (FWHM) of the signal from single adenovirus particles (n=236). The procedure was identical to that described previously (Wang et al., 2013).

Live imaging and data analyses

The live acquisition of fluorescent HAdV-C2 in infected cells was conducted by spinning disc confocal microscopy, essentially as described previously (Burckhardt et al., 2011). A customized Olympus IX81 inverted microscope (Olympus, Switzerland) was equipped with a Yokogawa scanning head QLC100 (VisiTech International, UK), with triple band-pass excitation (488 nm, 565 nm and 647 nm) and emission filters (Chroma, USA), and a temperature-controlled incubation box (Life Imaging Services, Basel, Switzerland). The fluorophores were excited by an Innova 70C mixed gas laser (Coherent, Germany), and the images recorded through an UPlanApo 100× immersion objective (numerical aperture 1.35; Olympus Optical AG, Switzerland) on a Cascade 512B EM-CCD camera (Photometrics, USA).

Image time series were recorded between 30 and 90 mpi. For imaging, infected cells were incubated in Hank’s buffered salt solution (Gibco-BRL) supplemented with 0.5% BSA and 1 mg/ml ascorbate at pH 7.3. HAdV-C2 labeled with either Atto565 or Alexa Fluor 488 was imaged at a frequency of 25 frames per second (Hz) for 5000 frames. The nuclear membrane, which was indicated by DRAQ5 DNA staining in TC7 cells or by rPOM121–EGFP3 expression in HeLa cells, was acquired in parallel to virion imaging for the same duration but at a lower frequency of 0.5 frames per second (Hz). The videos were processed with a single-particle-tracking program to obtain the 2D trajectories of cytoplasmic virions (Sbalzarini and Koumoutsakos, 2005). The accuracy of the virion position was estimated to be 20–50 nm according to a signal-to-noise ratio of 2.5 in the videos (Sbalzarini and Koumoutsakos, 2005). The trajectories of virus particles were processed with a trajectory segmentation algorithm using Support Vector Machines (SVM) as classifiers (Helmuth et al., 2007). The SVM was trained to classify segments of trajectories into four categories: microtubule-dependent directed motions (DM) and fast drifts (FD), microtubule-independent confined motions (CM) and slow drifts (SD), and unclassified stretches of trajectories were designated not-classified motions (NC), as described previously (Burckhardt et al., 2011; Engelke et al., 2011). Trajectories and segments were analyzed as described previously (Burckhardt et al., 2011). To detect the outline of the nucleus, images of DRAQ5 DNA staining or rPOM121–EGFP3 were thresholded using Otsu’s method to generate binary

images (Otsu, 1979). Since the boundaries of binary DRAQ5 and rPOM121–EGFP3 images correlated well with each other, both signals were taken as valid indicators of the nuclear membrane, which was subsequently employed to determine the subcellular localization of virus motions.

Image and data analysis

All the analyses were conducted on the raw images. Processing, analysis, data mining and visualization were performed using CellProfiler (Broad Institute, Cambridge, MA) and in-house MATLAB scripts (MathWorks Inc., Natick, MA, USA). Deconvolution of the image stacks was performed with AutoQuant (Media Cybernetics, Inc., Rockville, MD). The software for single particle tracking and trajectory segmentation is available from the website of the Sbalzarini laboratory (http://mosaic.mpi-cbg.de/?q=downloads/toolbox_for_particle_tracking; http://mosaic.mpi-cbg.de/?q=downloads/trajectory_segmentation). Source code used in this study is available upon request.

Acknowledgements

We thank Ralph Kehlenbach (University of Göttingen, Germany) for the gift of CRM1-C528S and discussions, Sten Strunze (University of Zurich) for instrumental support at the beginning of the project, Martin Engelke (University of Zurich) for help with virus motion analysis and discussion, Urs Ziegler and Jana Döhner (Center for Microscopy, University of Zurich) for the help with gSTED microscopy, and Maarit Suomalainen for valuable comments on the manuscript and discussions.

Competing interests

The authors declare no competing or financial interests.

Author contributions

Conceptualization: C.J.B., U.F.G.; Methodology: I.-H.W., C.J.B., A.Y., M.K.M.; Software: C.J.B., M.K.M.; Validation: I.-H.W., C.J.B., A.Y.; Formal analysis: I.-H.W., C.J.B., A.Y.; Investigation: I.-H.W., C.J.B., A.Y., U.F.G.; Resources: U.F.G.; Writing - original draft: I.-H.W., C.J.B., U.F.G.; Writing - review & editing: I.-H.W., C.J.B., U.F.G.; Visualization: I.-H.W., C.J.B., A.Y.; Supervision: U.F.G.; Project administration: U.F.G.; Funding acquisition: U.F.G.

Funding

This work was financed by a grant from the Swiss National Science Foundation to U.F.G. (310030B_160316), an instrument grant for gSTED super-resolution microscopy from the Swiss National Science Foundation to U.F.G. (R'Equip 316030_145037), and a scholarship from the Taiwanese government (Ministry of Education) to I.-H.W.

Data availability

The image and movie data, and source code for custom scripts used in this study is available upon request.

Supplementary information

Supplementary information available online at
http://jcs.biologists.org/lookup/doi/10.1242/jcs.203794.supplemental

References

Amstutz, B., Gastaldelli, M., Kälin, S., Imelli, N., Boucke, K., Wandeler, E., Mercer, J., Hemmi, S. and Greber, U. F. (2008). Subversion of CtBP1 controlled macropinocytosis by human Adenovirus serotype 3. *EMBO J.* **27**, 956-966.

Arhel, N., Genovesio, A., Kim, K.-A., Miko, S., Perret, E., Olivo-Marin, J.-C., Shorte, S. and Charneau, P. (2006). Quantitative four-dimensional tracking of cytoplasmic and nuclear HIV-1 complexes. *Nat. Methods* **3**, 817-824.

Aydin, I. and Schelhaas, M. (2016). Viral genome tethering to host cell chromatin: cause and consequences. *Traffic* **17**, 327-340.

Becskei, A. and Mattaj, I. W. (2003). The strategy for coupling the RanGTP gradient to nuclear protein export. *Proc. Natl. Acad. Sci. USA* **100**, 1717-1722.

Berk, A. J. (2007). Adenoviridae: the viruses and their replication. In *Fields Virology*, Vol. 2 (ed. D. M. Knipe and P. M. Howley), pp. 2355-2436. Philadelphia, PA, USA: Lippincott Williams & Wilkins.

Bremner, K. H., Scherer, J., Yi, J., Vershinin, M., Gross, S. P. and Vallee, R. B. (2009). Adenovirus transport via direct interaction of cytoplasmic dynein with the viral capsid hexon subunit. *Cell Host Microbe* **6**, 523-535.

Bruder, J. T. and Kovesdi, I. (1997). Adenovirus infection stimulates the Raf/Mapk signaling pathway and induces interleukin-8 expression. *J. Virol.* **71**, 398-404.

Burckhardt, C. J., Suomalainen, M., Schoenenberger, P., Boucke, K., Hemmi, S. and Greber, U. F. (2011). Drifting motions of the adenovirus receptor CAR and immobile integrins initiate virus uncoating and membrane lytic protein exposure. *Cell Host Microbe* **10**, 105-117.

Cassany, A., Ragues, J., Guan, T., Begu, D., Wodrich, H., Kann, M., Nemerow, G. R. and Gerace, L. (2014). Nuclear import of adenovirus DNA involves direct interaction of hexon with an N-terminal domain of the nucleoporin Nup214. *J. Virol.* **89**, 1719-1730.

Daelemans, D., Costes, S. V., Lockett, S. and Pavlakis, G. N. (2005). Kinetic and molecular analysis of nuclear export factor CRM1 association with its cargo in vivo. *Mol. Cell. Biol.* **25**, 728-739.

Daigle, N., Beaudouin, J., Hartnell, L., Imreh, G., Hallberg, E., Lippincott-Schwartz, J. and Ellenberg, J. (2001). Nuclear pore complexes form immobile networks and have a very low turnover in live mammalian cells. *J. Cell Biol.* **154**, 71-84.

Dodding, M. P. and Way, M. (2011). Coupling viruses to dynein and kinesin-1. *EMBO J.* **30**, 3527-3539.

Ekstrand, M. I., Enquist, L. W. and Pomeranz, L. E. (2008). The alpha-herpesviruses: molecular pathfinders in nervous system circuits. *Trends Mol. Med.* **14**, 134-140.

Engelke, M. F., Burckhardt, C. J., Morf, M. K. and Greber, U. F. (2011). The dynactin complex enhances the speed of microtubule-dependent motions of adenovirus both towards and away from the nucleus. *Viruses* **3**, 233-253.

Engelsma, D., Bernad, R., Calafat, J. and Fornerod, M. (2004). Supraphysiological nuclear export signals bind CRM1 independently of RanGTP and arrest at Nup358. *EMBO J.* **23**, 3643-3652.

Ewers, H., Smith, A. E., Sbalzarini, I. F., Lilie, H., Koumoutsakos, P. and Helenius, A. (2005). Single-particle tracking of murine polyoma virus-like particles on live cells and artificial membranes. *Proc. Natl. Acad. Sci. USA* **102**, 15110-15115.

Fallaux, F. J., Kranenburg, O., Cramer, S. J., Houweling, A., van Ormondt, H., Hoeben, R. C. and van der Eb, A. J. (1996). Characterization of 911: a new helper cell line for the titration and propagation of early region 1-deleted adenoviral vectors. *Hum. Gene. Ther.* **7**, 215-222.

Fornerod, M., Ohno, M., Yoshida, M. and Mattaj, I. W. (1997a). CRM1 is an export receptor for leucine-rich nuclear export signals. *Cell* **90**, 1051-1060.

Fornerod, M., van Deursen, J., van Baal, S., Reynolds, A., Davis, D., Murti, K. G., Fransen, J. and Grosveld, G. (1997b). The human homologue of yeast CRM1 is in a dynamic subcomplex with CAN/Nup214 and a novel nuclear pore component Nup88. *EMBO J.* **16**, 807-816.

Friedman, J. R., Webster, B. M., Mastronarde, D. N., Verhey, K. J. and Voeltz, G. K. (2010). ER sliding dynamics and ER-mitochondrial contacts occur on acetylated microtubules. *J. Cell Biol.* **190**, 363-375.

Gastaldelli, M., Imelli, N., Boucke, K., Amstutz, B., Meier, O. and Greber, U. F. (2008). Infectious adenovirus type 2 transport through early but not late endosomes. *Traffic* **9**, 2265-2278.

Gazzola, M., Burckhardt, C. J., Bayati, B., Engelke, M., Greber, U. F. and Koumoutsakos, P. (2009). A stochastic model for microtubule motors describes the in vivo cytoplasmic transport of human adenovirus. *PLoS Comput. Biol.* **5**, e1000623.

Giannakakou, P., Nakano, M., Nicolaou, K. C., O'Brate, A., Yu, J., Blagosklonny, M. V., Greber, U. F. and Fojo, T. (2002). Enhanced microtubule-dependent trafficking and p53 nuclear accumulation by suppression of microtubule dynamics. *Proc. Natl. Acad. Sci. USA* **99**, 10855-10860.

Görlich, D., Seewald, M. J. and Ribbeck, K. (2003). Characterization of Ran-driven cargo transport and the RanGTPase system by kinetic measurements and computer simulation. *EMBO J.* **22**, 1088-1100.

Greber, U. F. and Way, M. (2006). A superhighway to virus infection. *Cell* **124**, 741-754.

Greber, U. F., Willetts, M., Webster, P. and Helenius, A. (1993). Stepwise dismantling of adenovirus 2 during entry into cells. *Cell* **75**, 477-486.

Greber, U. F., Suomalainen, M., Stidwill, R. P., Boucke, K., Ebersold, M. W. and Helenius, A. (1997). The role of the nuclear pore complex in adenovirus DNA entry. *EMBO J.* **16**, 5998-6007.

Greber, U. F., Nakano, M. Y. and Suomalainen, M. (1998). Adenovirus entry into cells: a quantitative fluorescence microscopy approach. In *Adenovirus Methods and Protocols, in Meth. Mol. Med.*, Vol. 21 (ed. W. S. M. Wold), pp. 217-230. Totowa, NJ, USA: Humana Press, Inc.

Gross, S. P. (2004). Hither and yon: a review of bi-directional microtubule-based transport. *Phys. Biol.* **1**, R1-R11.

Helmuth, J. A., Burckhardt, C. J., Koumoutsakos, P., Greber, U. F. and Sbalzarini, I. F. (2007). A novel supervised trajectory segmentation algorithm identifies distinct types of human adenovirus motion in host cells. *J. Struct. Biol.* **159**, 347-358.

Hilliard, M., Frohnert, C., Spillner, C., Marcone, S., Nath, A., Lampe, T., Fitzgerald, D. J. and Kehlenbach, R. H. (2010). The anti-inflammatory prostaglandin 15-deoxy-delta(12,14)-PGJ2 inhibits CRM1-dependent nuclear protein export. *J. Biol. Chem.* **285**, 22202-22210.

Hsieh, M. J., White, P. J. and Pouton, C. W. (2010). Interaction of viruses with host cell molecular motors. *Curr. Opin. Biotechnol.* **21**, 633-639.

Hutten, S. and Kehlenbach, R. H. (2006). Nup214 is required for CRM1-dependent nuclear protein export in vivo. *Mol. Cell. Biol.* **26**, 6772-6785.

Hutten, S. and Kehlenbach, R. H. (2007). CRM1-mediated nuclear export: to the pore and beyond. *Trends Cell Biol.* **17**, 193-201.

Hyman, A. A., Weber, C. A. and Jülicher, F. (2014). Liquid-liquid phase separation in biology. *Annu. Rev. Cell Dev. Biol.* **30**, 39-58.

Imelli, N., Ruzsics, Z., Puntener, D., Gastaldelli, M. and Greber, U. F. (2009). Genetic reconstitution of the human adenovirus type 2 temperature-sensitive 1 mutant defective in endosomal escape. *Virol. J.* **6**, 174.
Janke, C. (2014). The tubulin code: molecular components, readout mechanisms, and functions. *J. Cell Biol.* **206**, 461-472.
Kaláb, P., Pralle, A., Isacoff, E. Y., Heald, R. and Weis, K. (2006). Analysis of a RanGTP-regulated gradient in mitotic somatic cells. *Nature* **440**, 697-701.
Kelkar, S. A., Pfister, K. K., Crystal, R. G. and Leopold, P. L. (2004). Cytoplasmic dynein mediates adenovirus binding to microtubules. *J. Virol.* **78**, 10122-10132.
Kelkar, S., De, B. P., Gao, G., Wilson, J. M., Crystal, R. G. and Leopold, P. L. (2006). A common mechanism for cytoplasmic dynein-dependent microtubule binding shared among adeno-associated virus and adenovirus serotypes. *J. Virol.* **80**, 7781-7785.
Kirli, K., Karaca, S., Dehne, H. J., Samwer, M., Pan, K. T., Lenz, C., Urlaub, H. and Görlich, D. (2015). A deep proteomics perspective on CRM1-mediated nuclear export and nucleocytoplasmic partitioning. *elife* **4**, e11466.
Kubo, T., Yanagisawa, H. A., Yagi, T., Hirono, M. and Kamiya, R. (2010). Tubulin polyglutamylation regulates axonemal motility by modulating activities of inner-arm dyneins. *Curr. Biol.* **20**, 441-445.
Kudo, N., Matsumori, N., Taoka, H., Fujiwara, D., Schreiner, E. P., Wolff, B., Yoshida, M. and Horinouchi, S. (1999). Leptomycin B inactivates CRM1/exportin 1 by covalent modification at a cysteine residue in the central conserved region. *Proc. Natl. Acad. Sci. USA* **96**, 9112-9117.
Leopold, P. L., Kreitzer, G., Miyazawa, N., Rempel, S., Pfister, K. K., Rodriguez-Boulan, E. and Crystal, R. G. (2000). Dynein- and microtubule-mediated translocation of adenovirus serotype 5 occurs after endosomal lysis. *Hum. Gene. Ther.* **11**, 151-165.
Li, J., Shariff, A., Wiking, M., Lundberg, E., Rohde, G. K. and Murphy, R. F. (2012). Estimating microtubule distributions from 2D immunofluorescence microscopy images reveals differences among human cultured cell lines. *PLoS ONE* **7**, e50292.
Lion, T. (2014). Adenovirus infections in immunocompetent and immunocompromised patients. *Clin. Microbiol. Rev.* **27**, 441-462.
Liu, H., Jin, L., Koh, S. B. S., Atanasov, I., Schein, S., Wu, L. and Zhou, Z. H. (2010). Atomic structure of human adenovirus by cryo-EM reveals interactions among protein networks. *Science* **329**, 1038-1043.
Luisoni, S., Suomalainen, M., Boucke, K., Tanner, L. B., Wenk, M. R., Guan, X. L., Grzybek, M., Coskun, U. and Greber, U. F. (2015). Co-option of membrane wounding enables virus penetration into cells. *Cell Host Microbe* **18**, 75-85.
Mabit, H., Nakano, M. Y., Prank, U., Saam, B., Dohner, K., Sodeik, B. and Greber, U. F. (2002). Intact microtubules support adenovirus and herpes simplex virus infections. *J. Virol.* **76**, 9962-9971.
Mahamid, J., Pfeffer, S., Schaffer, M., Villa, E., Danev, R., Cuellar, L. K., Forster, F., Hyman, A. A., Plitzko, J. M. and Baumeister, W. (2016). Visualizing the molecular sociology at the HeLa cell nuclear periphery. *Science* **351**, 969-972.
Marsh, M. and Helenius, A. (2006). Virus entry: open sesame. *Cell* **124**, 729-740.
McDonald, D., Vodicka, M. A., Lucero, G., Svitkina, T. M., Borisy, G. G., Emerman, M. and Hope, T. J. (2002). Visualization of the intracellular behavior of HIV in living cells. *J. Cell Biol.* **159**, 441-452.
Meier, O., Boucke, K., Hammer, S. V., Keller, S., Stidwill, R. P., Hemmi, S. and Greber, U. F. (2002). Adenovirus triggers macropinocytosis and endosomal leakage together with its clathrin-mediated uptake. *J. Cell Biol.* **158**, 1119-1131.
Mellman, I. and Warren, G. (2000). The road taken: past and future foundations of membrane traffic. *Cell* **100**, 99-112.
Moyer, C. L., Wiethoff, C. M., Maier, O., Smith, J. G. and Nemerow, G. R. (2011). Functional genetic and biophysical analyses of membrane disruption by human adenovirus. *J. Virol.* **85**, 2631-2641.
Nagel, H., Maag, S., Tassis, A., Nestlé, F. O., Greber, U. F. and Hemmi, S. (2003). The alphavbeta5 integrin of hematopoietic and nonhematopoietic cells is a transduction receptor of RGD-4C fiber-modified adenoviruses. *Gene Ther.* **10**, 1643-1653.
Nakano, M. Y., Boucke, K., Suomalainen, M., Stidwill, R. P. and Greber, U. F. (2000). The first step of adenovirus type 2 disassembly occurs at the cell surface, independently of endocytosis and escape to the cytosol. *J. Virol.* **74**, 7085-7095.
Napetschnig, J., Blobel, G. and Hoelz, A. (2007). Crystal structure of the N-terminal domain of the human protooncogene Nup214/CAN. *Proc. Natl. Acad. Sci. USA* **104**, 1783-1788.
Neville, M. and Rosbash, M. (1999). The NES-Crm1p export pathway is not a major mRNA export route in Saccharomyces cerevisiae. *EMBO J.* **18**, 3746-3756.
Otsu, N. (1979). A threshold selection method from gray-level histograms. *IEEE Trans. Syst. Man Cybern.* **9**, 62-66.
Piperno, G., LeDizet, M. and Chang, X. J. (1987). Microtubules containing acetylated alpha-tubulin in mammalian cells in culture. *J. Cell Biol.* **104**, 289-302.
Puntener, D., Engelke, M. F., Ruzsics, Z., Strunze, S., Wilhelm, C. and Greber, U. F. (2011). Stepwise loss of fluorescent core protein V from human adenovirus during entry into cells. *J. Virol.* **85**, 481-496.
Radtke, K., Dohner, K. and Sodeik, B. (2006). Viral interactions with the cytoskeleton: a hitchhiker's guide to the cell. *Cell. Microbiol.* **8**, 387-400.
Radtke, K., Kieneke, D., Wolfstein, A., Michael, K., Steffen, W., Scholz, T., Karger, A. and Sodeik, B. (2010). Plus- and minus-end directed microtubule motors bind simultaneously to herpes simplex virus capsids using different inner tegument structures. *PLoS Pathog.* **6**, e1000991.
Reddy, V. S., Natchiar, S. K., Stewart, P. L. and Nemerow, G. R. (2010). Crystal structure of human adenovirus at 3.5 A resolution. *Science* **329**, 1071-1075.
Reed, N. A., Cai, D., Blasius, T. L., Jih, G. T., Meyhofer, E., Gaertig, J. and Verhey, K. J. (2006). Microtubule acetylation promotes kinesin-1 binding and transport. *Curr. Biol.* **16**, 2166-2172.
Robinson, C. M., Singh, G., Lee, J. Y., Dehghan, S., Rajaiya, J., Liu, E. B., Yousuf, M. A., Betensky, R. A., Jones, M. S., Dyer, D. W. et al. (2013). Molecular evolution of human adenoviruses. *Sci. Rep.* **3**, 1812.
Sbalzarini, I. F. and Koumoutsakos, P. (2005). Feature point tracking and trajectory analysis for video imaging in cell biology. *J. Struct. Biol.* **151**, 182-195.
Scherer, J. and Vallee, R. B. (2011). Adenovirus recruits dynein by an evolutionary novel mechanism involving direct binding to pH-primed hexon. *Viruses* **3**, 1417-1431.
Schulze, E., Asai, D. J., Bulinski, J. C. and Kirschner, M. (1987). Posttranslational modification and microtubule stability. *J. Cell Biol.* **105**, 2167-2177.
Sirajuddin, M., Rice, L. M. and Vale, R. D. (2014). Regulation of microtubule motors by tubulin isotypes and post-translational modifications. *Nat. Cell Biol.* **16**, 335-344.
Smith, A. E., Slepchenko, B. M., Schaff, J. C., Loew, L. M. and Macara, I. G. (2002). Systems analysis of Ran transport. *Science* **295**, 488-491.
Smith, J. G., Cassany, A., Gerace, L., Ralston, R. and Nemerow, G. R. (2008). A neutralizing antibody blocks adenovirus infection by arresting microtubule-dependent cytoplasmic transport. *J. Virol.* **82**, 6492-6500.
Staufenbiel, M., Epple, P. and Deppert, W. (1986). Progressive reorganization of the host cell cytoskeleton during adenovirus infection. *J. Virol.* **60**, 1186-1191.
Strunze, S., Trotman, L. C., Boucke, K. and Greber, U. F. (2005). Nuclear targeting of adenovirus type 2 requires CRM1-mediated nuclear export. *Mol. Biol. Cell* **16**, 2999-3009.
Strunze, S., Engelke, M. F., Wang, I.-H., Puntener, D., Boucke, K., Schleich, S., Way, M., Schoenenberger, P., Burckhardt, C. J. and Greber, U. F. (2011). Kinesin-1-mediated capsid disassembly and disruption of the nuclear pore complex promote virus infection. *Cell Host Microbe* **10**, 210-223.
Sun, Q., Carrasco, Y. P., Hu, Y., Guo, X., Mirzaei, H., MacMillan, J. and Chook, Y. M. (2013). Nuclear export inhibition through covalent conjugation and hydrolysis of Leptomycin B by CRM1. *Proc. Natl. Acad. Sci. USA* **110**, 1303-1308.
Suomalainen, M., Nakano, M. Y., Keller, S., Boucke, K., Stidwill, R. P. and Greber, U. F. (1999). Microtubule-dependent plus- and minus end-directed motilities are competing processes for nuclear targeting of adenovirus. *J. Cell Biol.* **144**, 657-672.
Suomalainen, M., Nakano, M. Y., Boucke, K., Keller, S. and Greber, U. F. (2001). Adenovirus-activated PKA and p38/MAPK pathways boost microtubule-mediated nuclear targeting of virus. *EMBO J.* **20**, 1310-1319.
Suomalainen, M., Luisoni, S., Boucke, K., Bianchi, S., Engel, D. A. and Greber, U. F. (2013). A direct and versatile assay measuring membrane penetration of adenovirus in single cells. *J. Virol.* **87**, 12367-12379.
Taylor, M. P., Koyuncu, O. O. and Enquist, L. W. (2011). Subversion of the actin cytoskeleton during viral infection. *Nat. Rev. Microbiol.* **9**, 427-439.
Thakar, K., Karaca, S., Port, S. A., Urlaub, H. and Kehlenbach, R. H. (2013). Identification of CRM1-dependent nuclear export cargos using quantitative mass spectrometry. *Mol. Cell. Proteomics* **12**, 664-678.
Tollefson, A. E., Scaria, A., Hermiston, T. W., Ryerse, J. S., Wold, L. J. and Wold, W. S. (1996). The adenovirus death protein (E3-11.6K) is required at very late stages of infection for efficient cell lysis and release of adenovirus from infected cells. *J. Virol.* **70**, 2296-2306.
Trobridge, G. D. (2009). Foamy virus vectors for gene transfer. *Expert Opin Biol. Ther.* **9**, 1427-1436.
Trotman, L. C., Mosberger, N., Fornerod, M., Stidwill, R. P. and Greber, U. F. (2001). Import of adenovirus DNA involves the nuclear pore complex receptor CAN/Nup214 and histone H1. *Nat. Cell Biol.* **3**, 1092-1100.
Verhey, K. J. and Gaertig, J. (2007). The tubulin code. *Cell Cycle* **6**, 2152-2160.
Verkman, A. S. (2002). Solute and macromolecule diffusion in cellular aqueous compartments. *Trends Biochem. Sci.* **27**, 27-33.
Wang, I.-H., Suomalainen, M., Andriasyan, V., Kilcher, S., Mercer, J., Neef, A., Luedtke, N. W. and Greber, U. F. (2013). Tracking viral genomes in host cells at single-molecule resolution. *Cell Host Microbe* **14**, 468-480.
Warren, J. C. and Cassimeris, L. (2007). The contributions of microtubule stability and dynamic instability to adenovirus nuclear localization efficiency. *Cell Motil. Cytoskeleton* **64**, 675-689.
Warren, J. C., Rutkowski, A. and Cassimeris, L. (2006). Infection with replication-deficient adenovirus induces changes in the dynamic instability of host cell microtubules. *Mol. Biol. Cell* **17**, 3557-3568.
Welte, M. A. (2004). Bidirectional transport along microtubules. *Curr. Biol.* **14**, R525-R537.
Wolfrum, N. and Greber, U. F. (2013). Adenovirus signalling in entry. *Cell. Microbiol.* **15**, 53-62.
Xu, D., Marquis, K., Pei, J., Fu, S.-C., Cagatay, T., Grishin, N. V. and Chook, Y. M. (2015). LocNES: a computational tool for locating classical NESs in CRM1 cargo proteins. *Bioinformatics* **31**, 1357-1365.
Yamauchi, Y. and Greber, U. F. (2016). Principles of virus uncoating: cues and the snooker ball. *Traffic* **17**, 569-592.
Zemp, I., Wild, T., O'Donohue, M.-F., Wandrey, F., Widmann, B., Gleizes, P.-E. and Kutay, U. (2009). Distinct cytoplasmic maturation steps of 40S ribosomal subunit precursors require hRio2. *J. Cell Biol.* **185**, 1167-1180.

Supplementary Data

The nuclear export factor CRM1 controls juxta-nuclear microtubule-dependent virus transport

I-Hsuan Wang, Christoph J. Burckhardt, Artur Yakimovich, Matthias K. Morf & Urs F. Greber

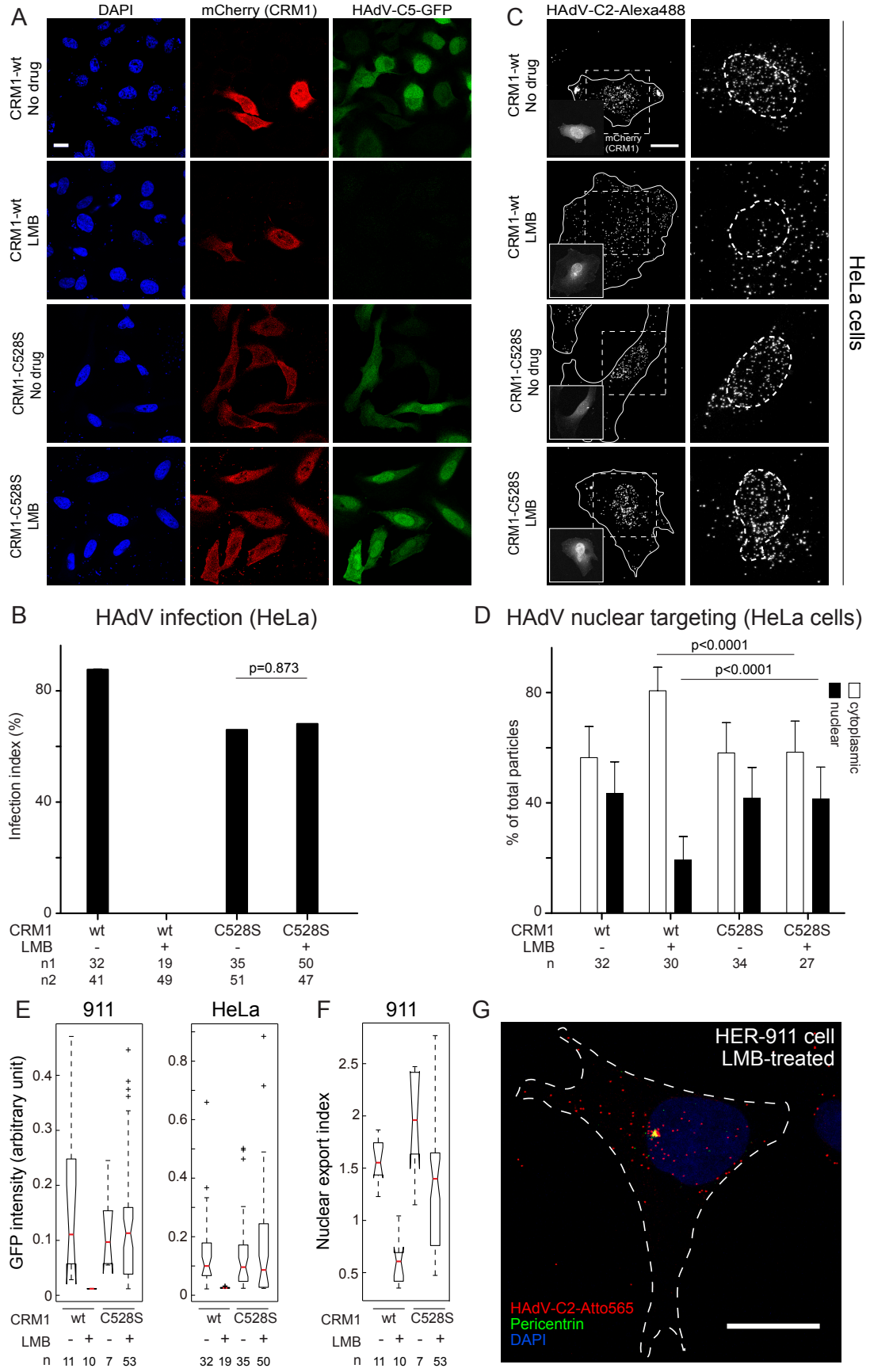

Fig. S1: Rescue of adenovirus nuclear targeting and genome delivery in LMB-treated HeLa and HER-911 cells expressing LMB-resistant CRM1 (related to Fig. 1).

A) HeLa cells were transfected with CRM1-wt-mCherry or CRM1-C528S-mCherry and treated with or without LMB, followed by inoculation of HAdV-C5_GFP for 16 h. Scale bar = 20 µm.

B) Representation of infection indexes based on the percentage of infected (GFP positive) transfected cells, including the p-value between LMB and control cells transfected with the LMB resistant mutant CRM1-C528S-mCherry. The experiment was conducted twice, and the numbers of cells analyzed in each biological replicate are indicated (n1, n2).

C) Examination of the nuclear targeting of incoming HAdV-C2-Atto647 particles in CRM1-wt-mCherry and CRM1-C528S-mCherry expressing HeLa cells 90 min pi. The transfected cells are displayed in the inset with white outline. The dashed lines in the blown-up images in the right row indicate the nuclear region. Scale bar = 20 µm.

D) Quantification of HAdV-C2-Atto647 nuclear targeting. Mean values of the subcellular localization of the virions at the nuclear membrane and in the cytoplasm, including the standard deviations and number of cells analyzed (n).

E) Representative data sets of HAdV-C5_GFP infections. The notched boxplots show the 25^{th} to 75^{th} percentile and median of data points. Outliers, which are 1.5 times the interquartile range (indicated by the whisker) away from the edge of the box, are represented by the plus signs.

F) Assessment of nuclear export of endogenous Rio2 in HER-911 cells transfected with CRM1-wt-mCherry or CRM1-C528S-mCherry, in presence or absence of LMB.

G) Representative image of incoming HAdV-C2-Atto565 particles arrested at MTOC upon LMB treatment in HER-911 cell 90 min pi. The MTOC was immunolabeled by an anti-pericentrin antibody. The dashed line indicates the outline of the cell. Scale bar = 20 µm.

Journal of Cell Science • Supplementary information

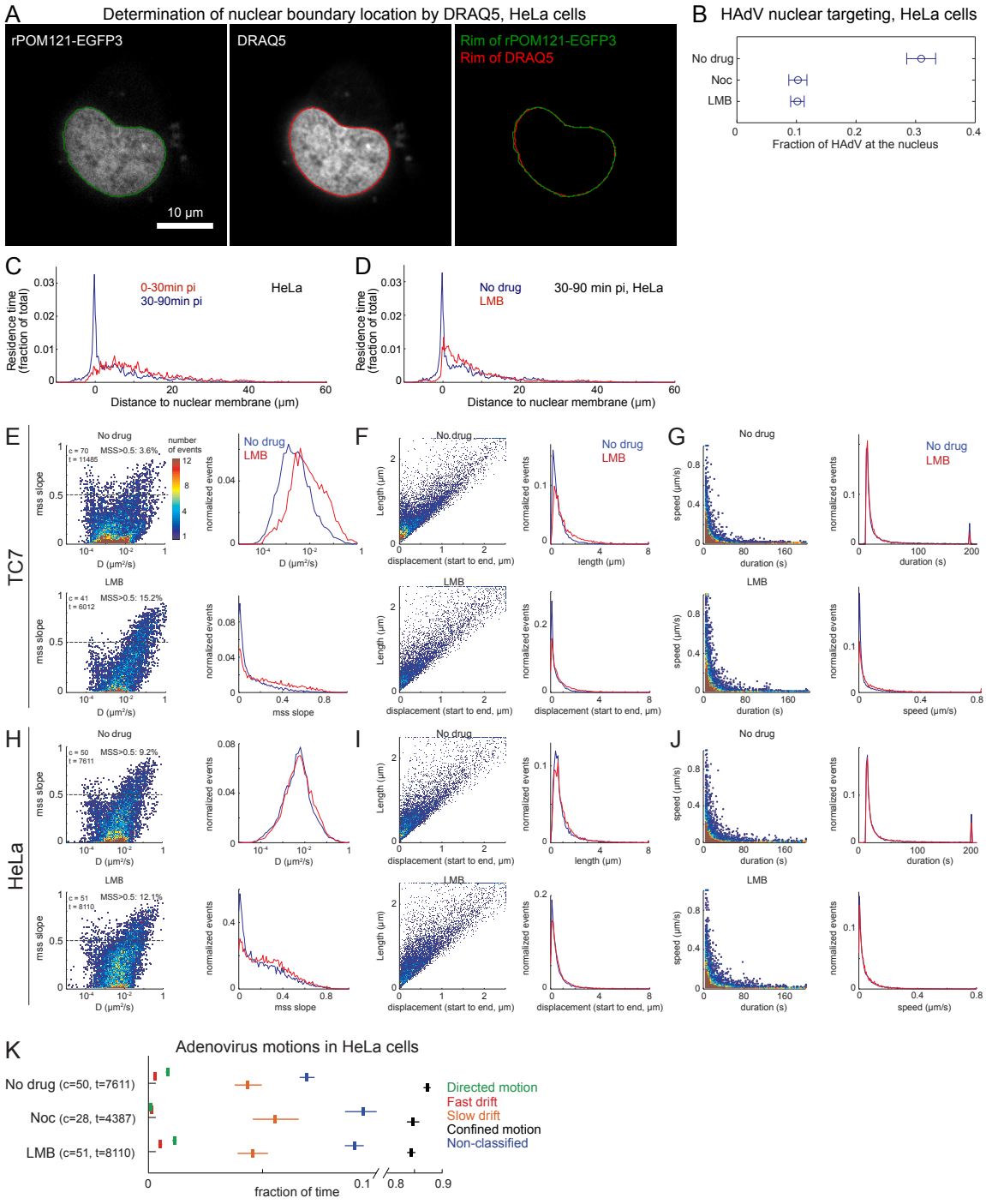

Fig. S2: Analyzing the subcellular localization of viruses by live cell imaging in HeLa and TC7 cells (related to Fig. 2).

A) To validate the delineation of the nuclear rim determined by DRAQ5 in fixed specimens, TC7 cells were transfected with rPOM121-EGFP3, and stained with DRAQ5 in live mode. The boundaries of the rPOM121-EGFP3 and DRAQ5 signals were

determined and compared with each other using the same procedures as for the fixed cells. The results show a high degree of overlap between the POM121 and the DRAQ5 nuclear rims.

B) Analyses of HAdV-C2-Alexa565 located at the nuclear membrane in HeLa cells upon treatment with LMB or nocodazole (Noc) 30-90 min pi.

C) Residence time of HAdV-C2-Alexa565 in relation to the distance of the virions from the nuclear membrane in the time windows 0-30 min and 30-90 min pi.

D) Distance plot of residence time of HAdV-C2-Alexa565 in presence or absence of LMB, 30-90 min pi.

E, F) Characterization of adenovirus movements in infected TC7 and HeLa cells by frequency plots of mss slopes and diffusion constants of virion trajectories, and histogram profiling in control cells (blue) and LMB-treated cells (red). Events with mss slopes >0.5 represent active transport, 0.5 random walk (dashed line), and <0.5 restricted diffusion. The number of cells (c) and virus tracks (t) analyzed are indicated for each panel.

G, H) Frequency plots of trajectory run lengths and overall displacements of virions. Note the indication of the relative occurrence of motion periods with an MSS-slope larger than 0.5, that is, with a high component of linear motion (panels E and H).

I, J) Frequency plots of speed and duration of virion movements.

K) Abolishment of adenovirus directed motions and fast drifts in HeLa cells by nocodazole. Representation of the median time, for which virions engaged in directed motion (DM, green), fast drift (FD, red), slow drift (SD, orange), diffusion (cyan), confined motions (CM, black) and not classified (NC, dark blue) including 95% confidence intervals (horizontal bars) obtained by bootstrapping. Results are expressed as a fraction of total time analyzed for each condition, and include the number of cells (c), and the number of virus trajectories (t).

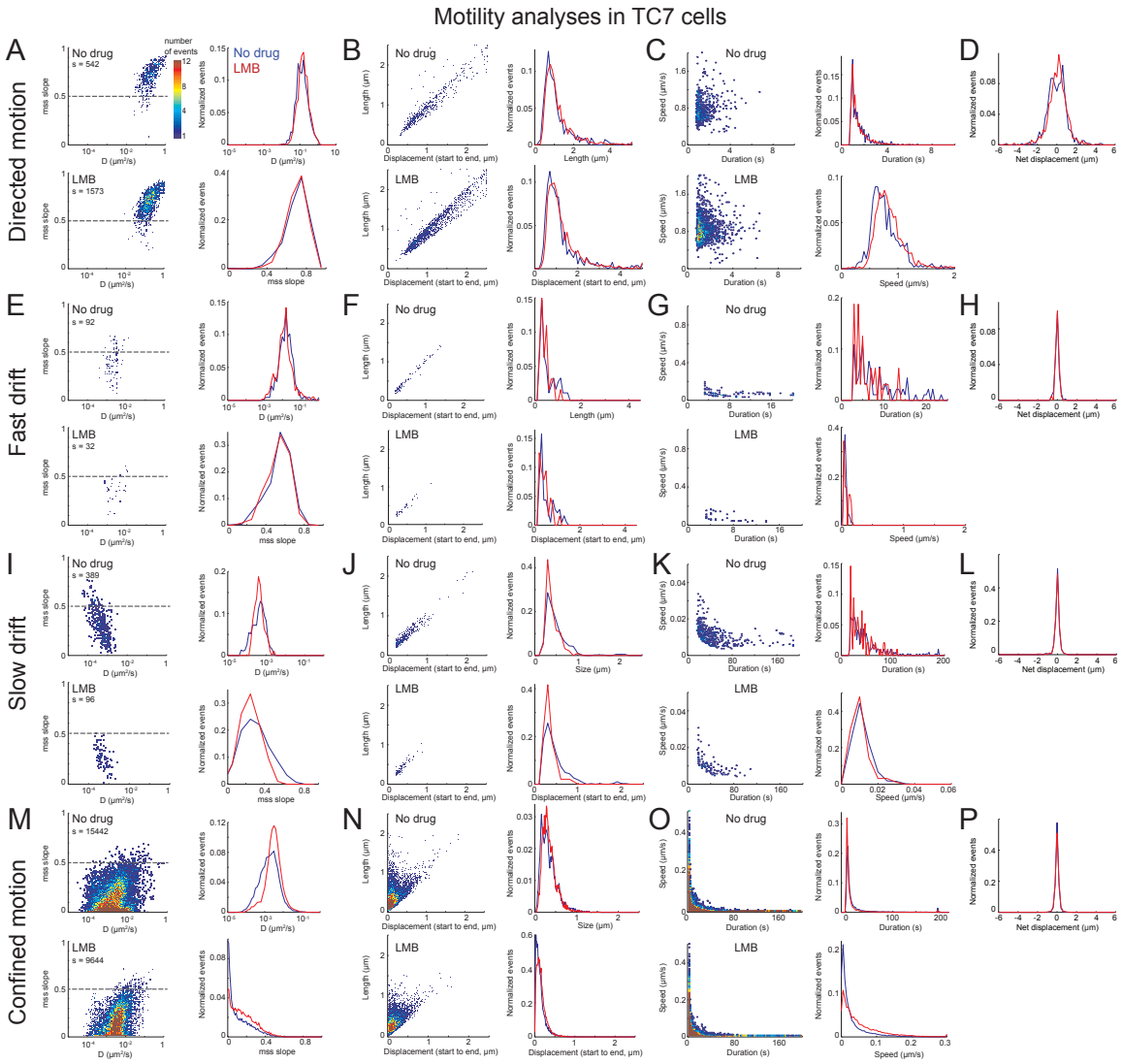

Fig. S3: Features of virion motions in TC7 cells (related to Fig. 2).

The virion trajectories from control and LMB-treated cells were segmented and categorized into directed motion (**A-D**), fast drift (**E-H**), slow drift (**I-L**), and confined motion (**M-P**). Each motion type was analyzed for its mss slope (**A, E, I, M**), run length (**B, F, J, N**), duration (**C, G, K, O**) and directionality (**D, H, L, P**). The distribution of these parameters was plotted and compared between control (blue) and LMB-treated cells (red), including the number of segments analyzed (s).

Journal of Cell Science • Supplementary information

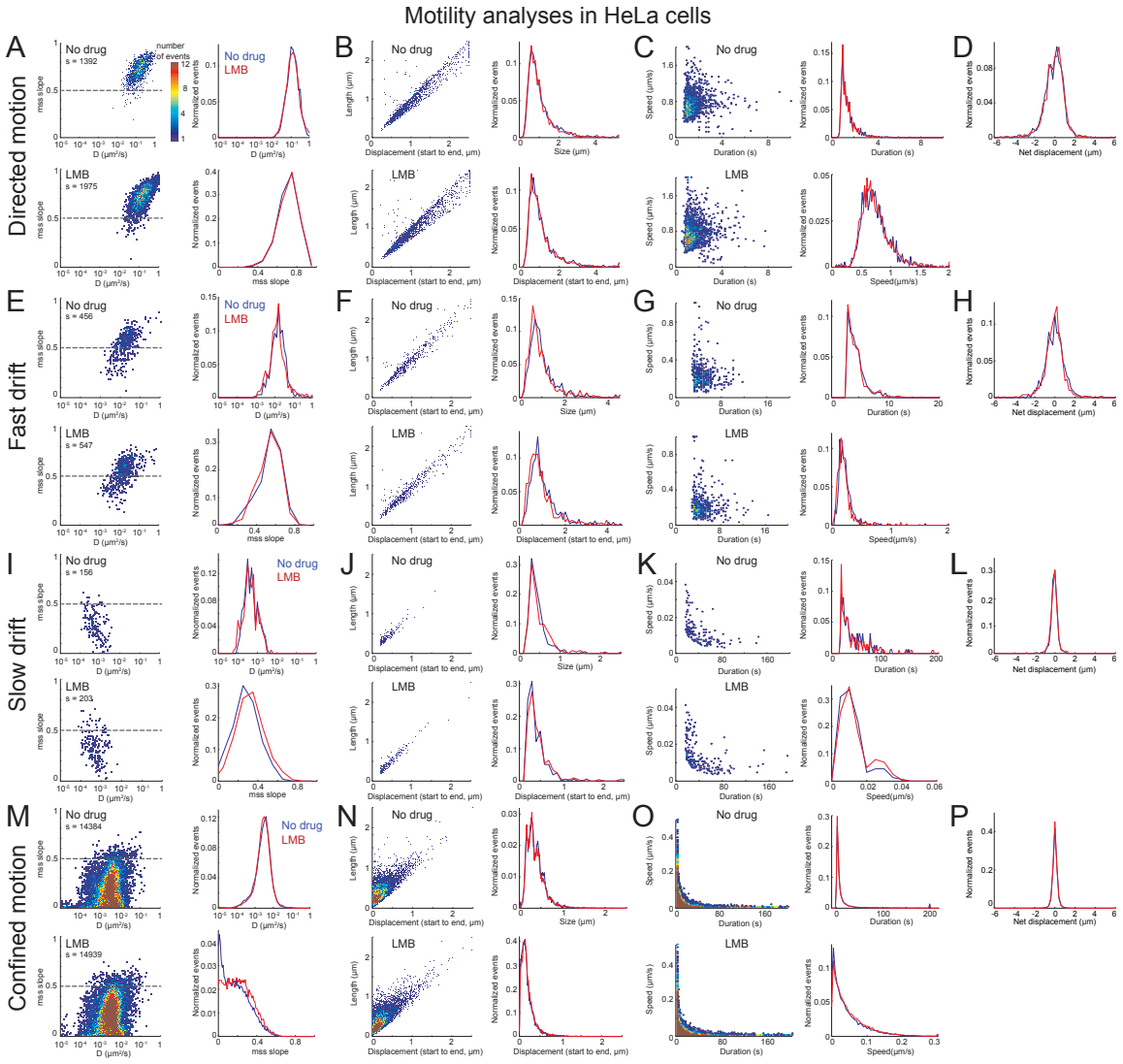

Fig. S4: Features of virion motions in HeLa cells (related to Fig. 2).

The virion trajectories from control and LMB-treated cells were segmented and categorized into directed motion (**A-D**), fast drift (**E-H**), slow drift (**I-L**), and confined motion (**M-P**). Each motion type was analyzed for its mss slope (**A, E, I, M**), run length (**B, F, J, N**), duration (**C, G, K, O**) and directionality (**D, H, L, P**). The distribution of these parameters was plotted and compared between control (blue) and LMB-treated cells (red), including the number of segments analyzed (s).

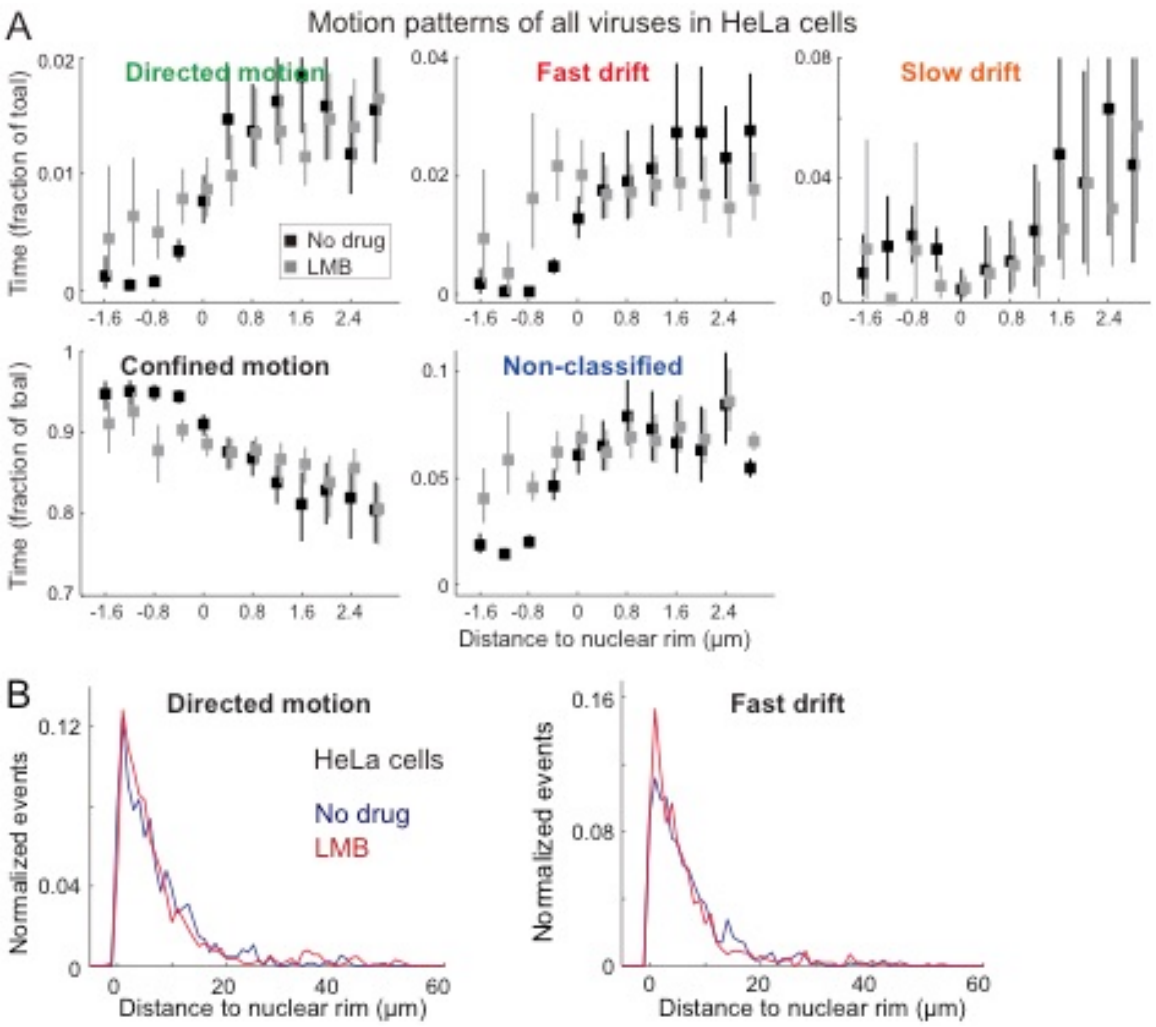

Fig. S5: CRM1-sensitive motion gradient of adenovirus in HeLa cells (related to Fig. 4).

A) Virion motions in relation to their distance from the nucleus in the zone -1.6 µm to 2.8 µm around the nuclear rim. The nuclear rim is positioned at 0. Negative distance values indicate overlap with the nuclear mask, and positive values indicate motions in the cytoplasm distant from the nucleus. Events were binned into 0.4 µm segments, and results plotted as the median time of virions in each motion type. Results from control cells are represented in black, and LMB-treated cells in grey squares.

B) Subcellular localization of the starting points of the DM and FD across the entire cytoplasm of control and LMB-treated cells.

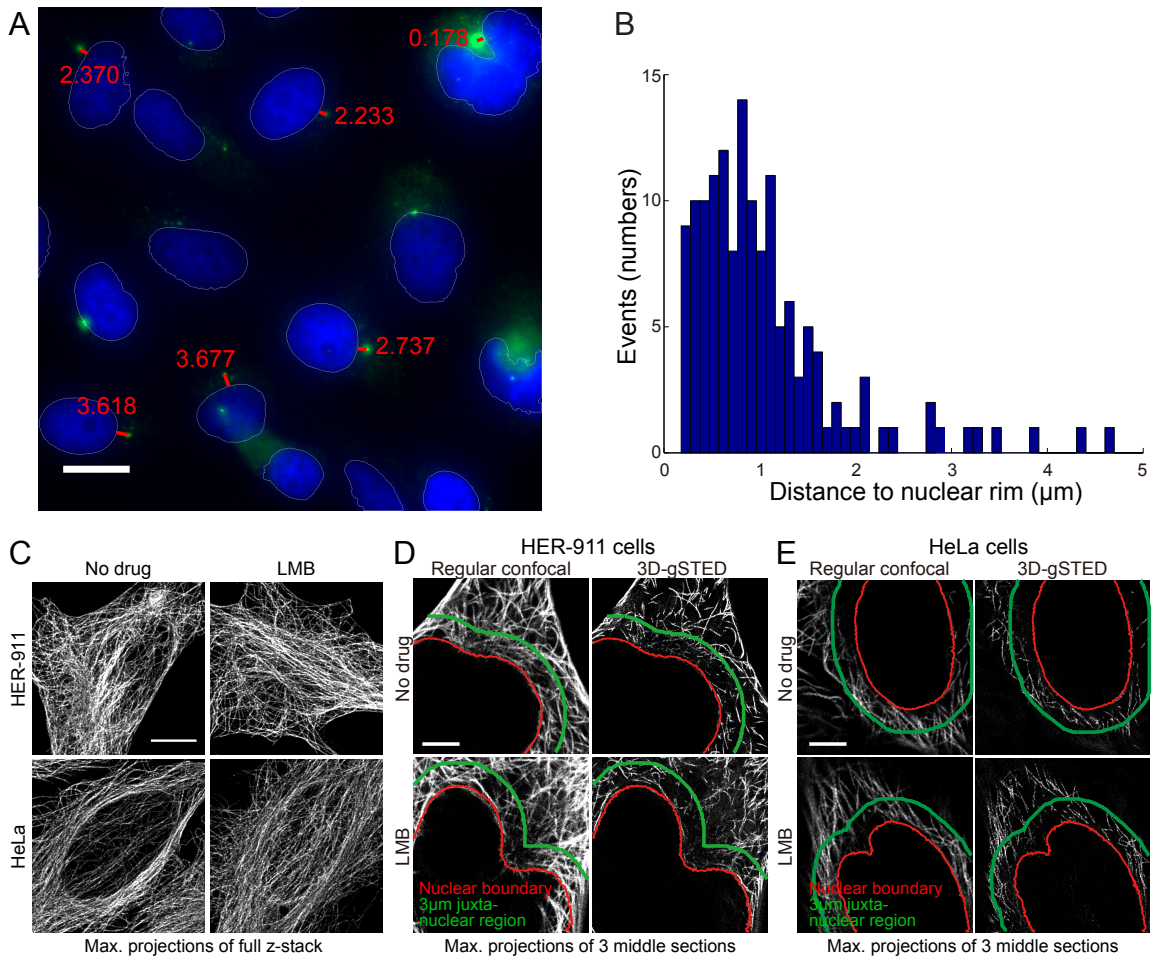

Fig. S6: Distance profiling of the location of the MTOC with respect to the nuclear membrane and microtubule morphology in the perinuclear zone (related to Fig. 5).

A) A representative image of the microtubule organizing centers (MTOCs) stained with an anti-pericentrin antibody (green), and DAPI-stained nuclei (blue) as a reference in HER-911 cells. The distance between the MTOC and the nuclear rim (white line) is indicated by a red line and a corresponding red number in μm. Scale bar: 20 μm.

B) Histogram showing the frequency of MTOC location with respect to the nuclear rim.

C) Morphology of the microtubule network in HER-911 and HeLa cells. Control or LMB-treated cells were stained for β-tubulin, imaged by confocal fluorescence microscopy, and displayed as maximal projections of deconvolved image stacks. Scale bar = 10 μm.

D, E) Three z-sections of microtubule-stained HER-911 (B) and HeLa (C) cells were acquired at the middle of the cells in 3D-gSTED mode of the confocal laser scanning microscope. The maximum projections were created from image stacks. Scale bar = 5 µm.

MovieS1

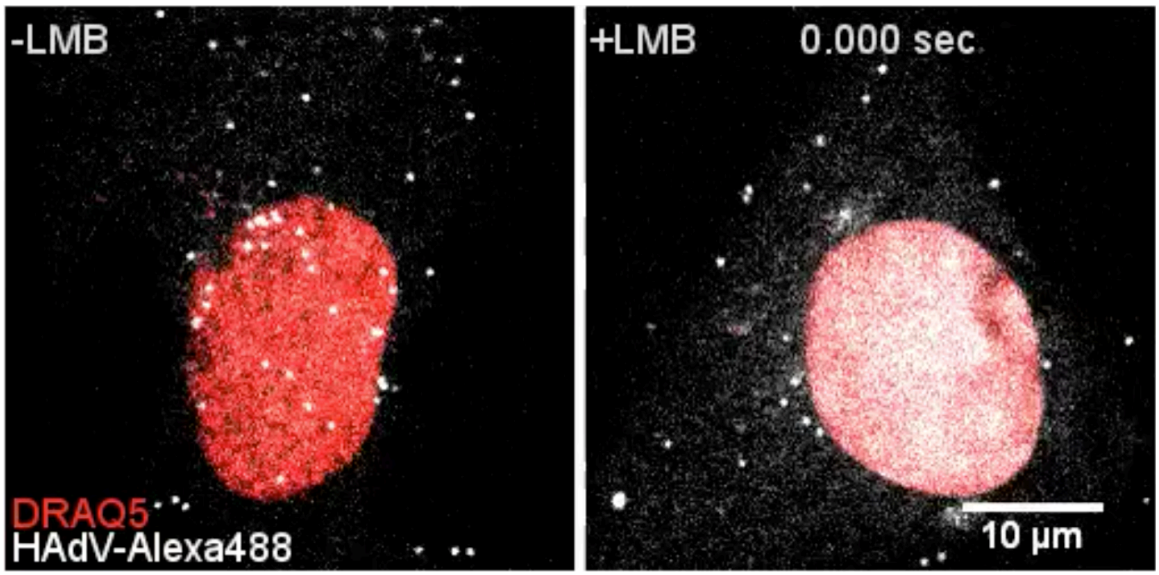

Supplementary Movie 1: Motility of adenovirus particles in control and LMB-treated TC7 cells.

Control or LMB-treated TC7 cells stained for DNA with DRAQ5 were warmed for 30-90 min from cold-synchronized inoculation of HAdV-C2-Alexa488 (white), and imaged by spinning disc confocal microscopy at a frequency of 25 Hz. For details about the procedure, see main text.